SECTION 97

THE EXTRAPOLATION OF LABORATORY AND AIRCRAFT RADAR SEA RETURN DATA TO SPACECRAFT ALTITUDES

by

Willard J. Pierson
Department of Meteorology and Oceanography
School of Engineering and Science
New York University

and

Richard K. Moore
Remote Sensing Laboratory
University of Kansas

ABSTRACT

Laboratory measurements show that the spectra of the capillary waves grow with wind speed over six orders of magnitude. Measurements in a wind-water tunnel show a simple one to one relationship between σ^{o}_{VV} and wind speed. The laboratory data for both waves and backscatter have negligible scatter because the wind for each measurement was constant and the radar return and wave spectra were averaged over a long enough time. Other conditions did not change.

Regression analyses of upwind and crosswind values of $10 \log_{10} (\overline{\sigma}^{o}(\theta)/\overline{\sigma}^{o}(10°))$ from aircraft data show linear relationships with the logarithm of the wind speed at 15°, 25° and 35°. The data have substantial scatter in part because both the average wind speed and average sea return values had to be estimated from relatively short samples. The scatter can be partially understood and predicted from a combination of turbulence theory, radar theory, and the small sampling theory of statistical inference. The scatter is caused in part by two effects; the turbulence of the wind over the water and the "fading" characteristics of the radar return.

When these results are applied to a prediction of the sea return values to be obtained by S193 on Skylab, it can be shown that the size of the illuminated patch effectively averages out the horizontal scales of gustiness so that the measurement will correspond to the synoptic scale wind. The effect of "fading" will introduce a scatter of less than six percent for angles greater than 15°.

There will still be some difficult problems to be solved for S193. These problems are described, and methods for their solution are reviewed.

INTRODUCTION

Both laboratory and aircraft measurements over the ocean increasingly support a strong correlation between radar sea return and wind velocity. It is dangerous to oversimplify the results obtained in the laboratory, and apply them directly to the open ocean without first accounting for differences between laboratory and open ocean conditions. However, once these differences are accounted for, the combined information obtained from the laboratory and from aircraft measurements makes it possible to understand some of the reasons for the scatter in the aircraft data and to calculate what these effects will be in the measurements to be made by S193 on Skylab. Such an analysis also reveals that only part of the scatter in the aircraft data is caused by sampling variability in the data. Reasons for this additional scatter are postulated. Many of these other sources of scatter will not be present in S193, and still others can be removed with the larger data base to be made available when Skylab is flown.

LABORATORY DATA

Laboratory data on the form of the capillary wave spectrum have been combined to show that the capillary spectrum in a wind-water tunnel varies over six orders of magnitude as shown by Pierson, Jackson, et al. (1971). In Figure 1, the capillary waves are very low below a friction velocity, u_*, of 10 or 12 cm/sec. Then the waves grow by more than four orders of magnitude as the friction velocity changes by just a few cm/sec. The spectrum still grows with increasing wind speed all the way to friction velocities of 150 cm/sec, but more slowly. Photographic data also support the conclusion that the spectrum grows with increasing wind speed in the capillary frequency range.

Wright has measured σ^{o}_{VV} at 60° off the vertical in a wind-water tunnel for a wide range of wind speeds. These values are the exact unnormalized values for the scattering cross section. Some of the preliminary results are shown in Figure 2. The backscatter from the capillary waves clearly increases with increasing wind speed. The change from a very steep slope to a less steep slope in this plot corresponds to the value D equals one in Figure 1. Wind speeds in the free air section of the tunnel are given in feet/min. An auxiliary scale gives

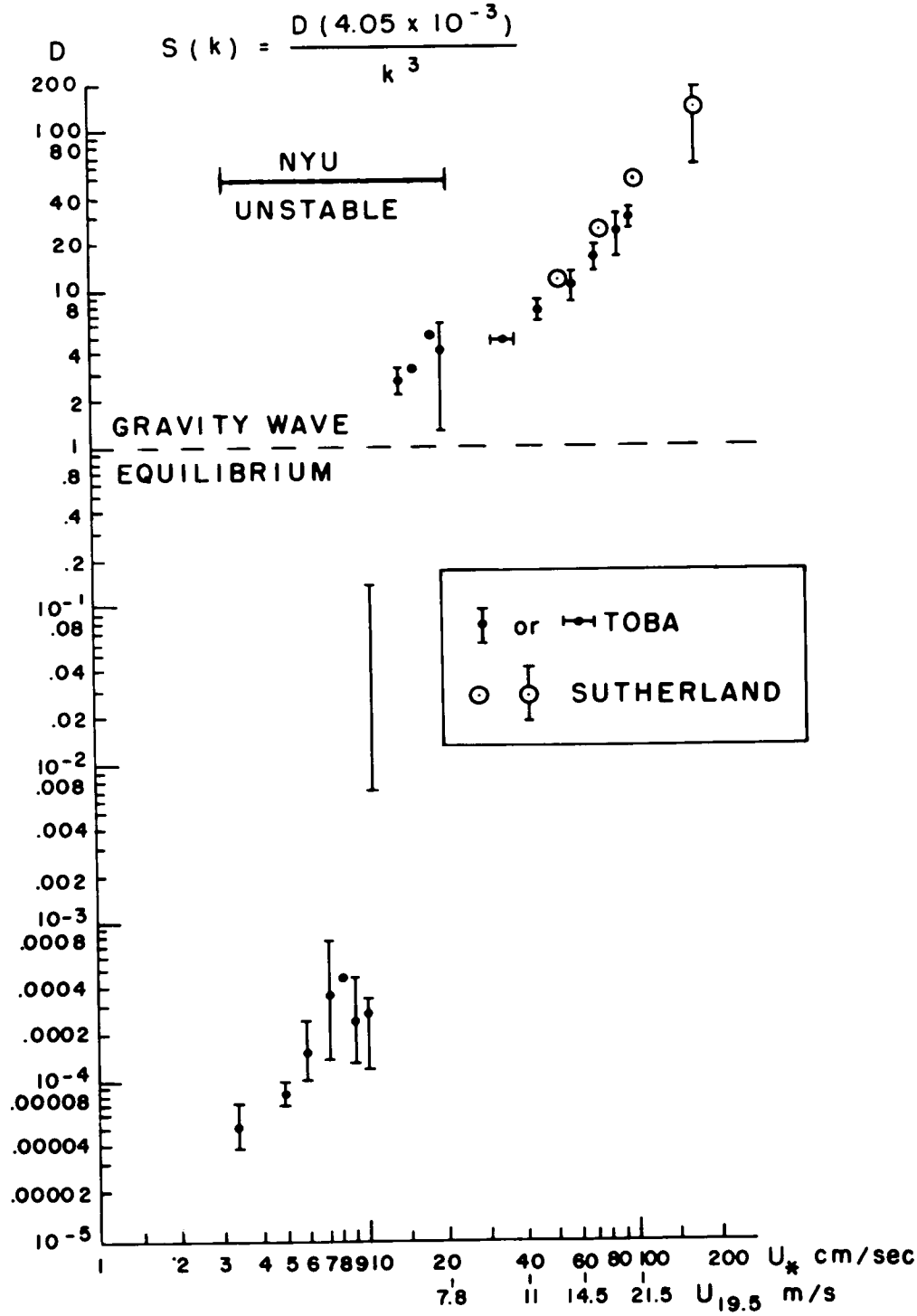

FIG. 1. VARIATION OF D AS A FUNCTION OF U_* IN THE CAPILLARY WAVE SPECTRUM.

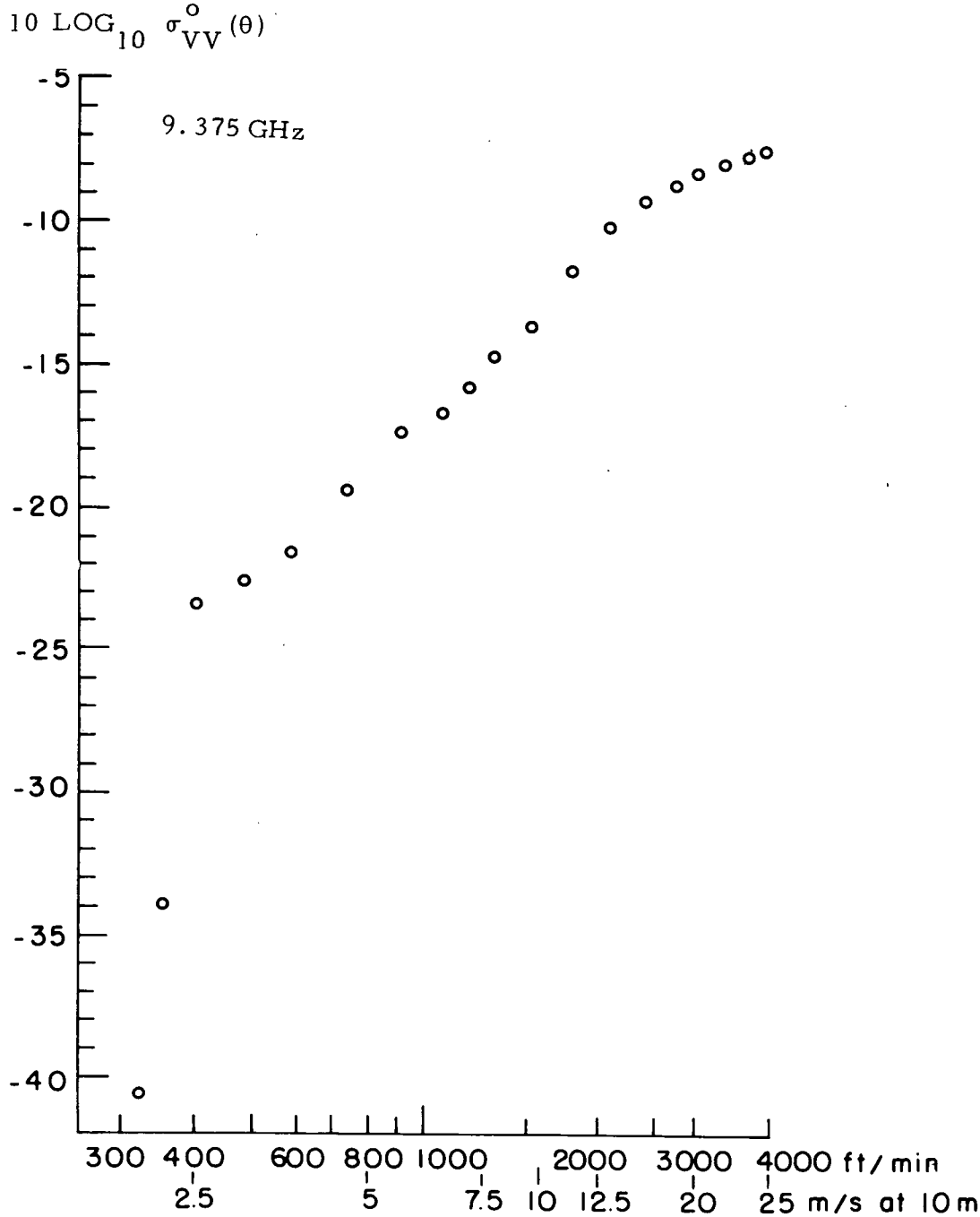

FIG. 2 RADAR BACKSCATTER AS A FUNCTION OF WIND SPEED IN A WIND-WATER TUNNEL. DATA COURTESY OF DR. JOHN WRIGHT.

the approximate equivalent wind at 10 meters over the ocean.

In experiments in wind-water tunnels, it is possible to keep conditions relatively simple compared to the open ocean. Measurements can be averaged over a sufficiently long time so as to ensure the elimination of sampling variability. Near the surface of the open ocean, wind speeds of the values shown would produce much larger waves, with a spectrum extending to much lower frequencies. Moreover, the winds over the ocean are not as steady as the winds in a wind-water tunnel.

ATMOSPHERIC TURBULENCE

The atmosphere is turbulent; its many scales of motion can be assigned to three categories; the microscale, the mesoscale and the macroscale, or the planetary scale. A wind vane and an anemometer respond to the frequencies in the microscale with some damping. The mesoscale is often unimportant over the oceans, but it is important for the study of, for example, mountain-valley winds, thunderstorms, and heat islands over cities.

Lumley and Panofsky (1964) cite an important paper by Van der Hoven (1957) that first attempted to study the full range of motions for the horizontal wind. A figure from Lumley and Panofsky (1964) which is redrawn from Van der Hoven (1957) is repeated here as Figure 3.

This figure is an oversimplification of the problem; yet the oversimplification provides an important insight into the nature of turbulence. The vertical scale is $n\,S(n)$ where n is the frequency and $S(n)$ is the variance spectrum of the wind with dimensions of $(\text{velocity})^2$ times time so that the vertical axis has the dimensions of $m^2\ sec^{-2}$. The horizontal scale is a logarithmic scale in n where n is in cycles per hour.

The graph has the property that

$$\int_{n_1}^{n_2} n\,S(n)\,d\log n = \int_{n_1}^{n_2} n\,S(n)\,\frac{dn}{n} = \int_{n_1}^{n_2} S(n)\,dn \qquad (1)$$

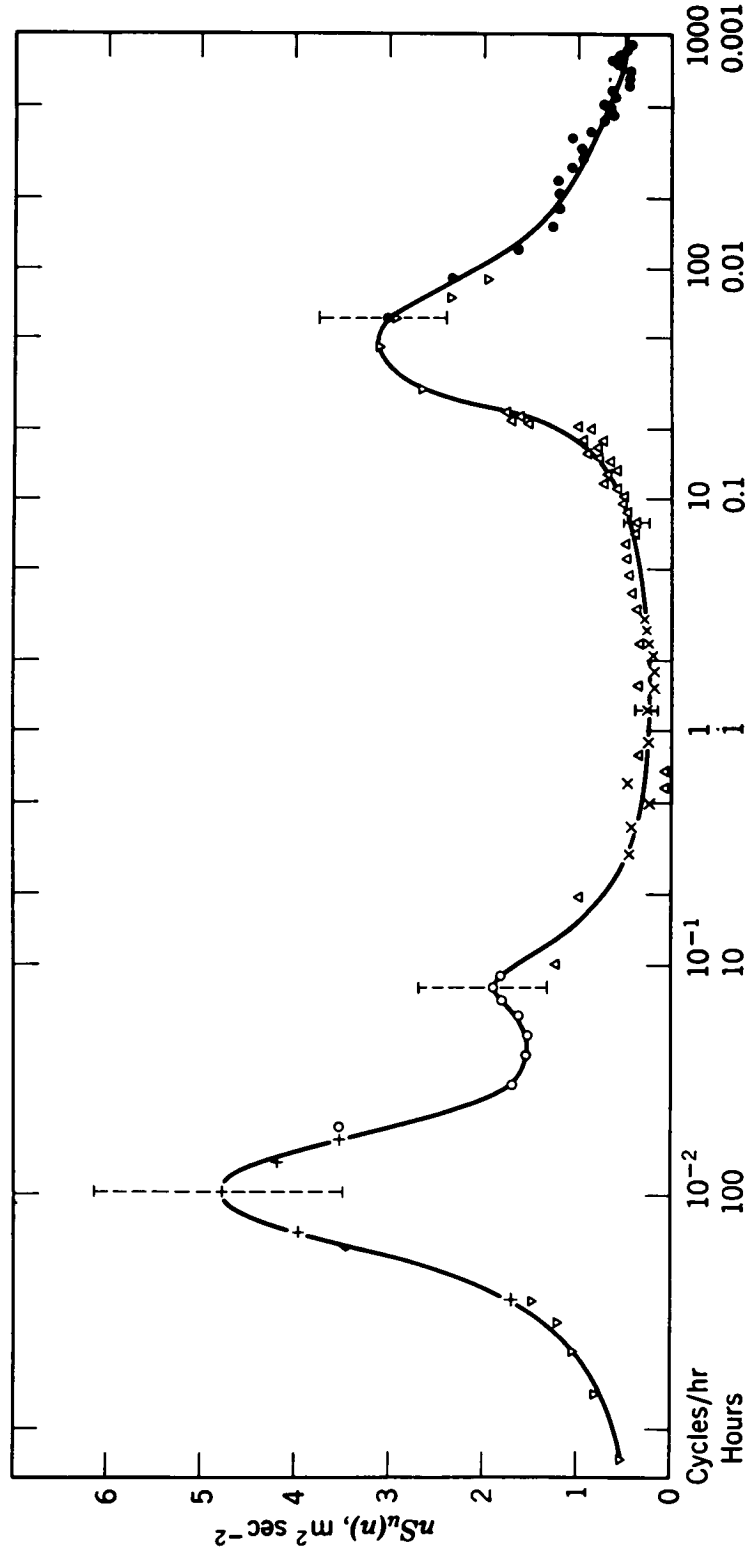

FIG. 3. Schematic spectrum of wind speed near the ground estimated from a study of Van der Hoven (1957).

(FROM LUMLEY AND PANOFSKY (1964), INTERSCIENCE, JOHN WILEY AND SONS).

so that this form preserves area in contrast to one where the logarithm of S(n) is plotted against the logarithm of n.

Figure 3 has three relative maxima; one near 50 cycles per hour, one near one cycle per twelve hours and one near one cycle per four days. The part on the left is typical of what might be computed for S(n) if say, the winds were recorded by an anemometer near the ground once an hour as one hour averages for a year or so and then the variance spectrum was computed. The part on the left would vary considerably from one place in the world to another.

The part on the right represents the spectrum of the gusts and lulls of the horizontal wind. It really depends to a very large extent on the speed and direction of the average planetary wind during the time the record was obtained from which the spectrum on the right side was computed. If the synoptic scale wind is high, the spectrum on the right will be high. If the wind is low, the spectrum will be low.

The usual anemometer installation is hardly the optimum instrumentation for the study of turbulence, but studies of turbulence with faster response instrumentation by Phelps and Pond (1971) and DeLeonibus (1971) show that simple anemometers yield useful information on the important scales of turbulence in the wind. Much of what was known through 1964 is summarized by Lumley and Panofsky (1964).

The important point about Figure 3 is not the three peaks in the spectrum, which fluctuate in amplitude and position, but the low region in the spectrum extending from about .05 to 10 cycles per hour. The area under the curve to the left of this band is five to six times greater than the area under the curve in the band. The area to the right is four to five times greater.

The low region in this spectrum justifies the fundamental hypothesis of numerical weather prediction; namely that the turbulent high frequency part of atmospheric motions can be filtered out of the synoptic scales, and parameterized as "eddy Austausch" coefficients so that numerical weather predictions can be carried out on a grid with spacings large compared to the scales of the eddies in the spectra on the right hand side. The numerical weather prediction schemes use functions of the synoptic scale winds that depend on a parameterization of the turbulence. The synoptic scale winds are nearly horizontal with the vertical components of the motion being 10^{-4} times the horizontal components.

If $\vec{V}(x, y, z, t)$ is the horizontal wind in the planetary boundary layer over the ocean, then

$$\bar{\vec{V}}(x, y, x, t) = \frac{1}{T} \int_{t-T/2}^{t+T/2} \vec{V}(x, y, z, t_o)\ dt_o \qquad (2)$$

and

$$\vec{V}(x, y, z, t) = \bar{\vec{V}}(x, y, z, t) + \vec{V}'(x, y, z, t) \qquad (3)$$

where

$$\vec{V}'(x, y, z, t) = \vec{V}(x, y, z, t) - \bar{\vec{V}}(x, y, z, t) \qquad (4)$$

The turbulence, that is the fluctuations in the wind to the right of, say, one cycle per half hour, is now in the $\vec{V}'$. The synoptic scale wind, in the absence of any important mesoscale perturbation, such as thunderstorms, is now the V.

Equally well, one could write equation 5 instead of equation 2 and substitute a space average for a time average where A is some area over the ocean surface.

$$\bar{\vec{V}}(x, y, z, t) = \frac{1}{A} \int_A \int \vec{V}(x_o, y_o, z, t)\ dx_o\ dy_o \qquad (5)$$

These concepts have been applied to a study of the best way to process anemometer data to be obtained by the National Data Buoy System of NOAA by Baer and Withee (1972a, 1972b). Numerous spectra similar to the one shown in Figure 3 for Argus Island, Keflavik, Iceland, and a site in the Pacific Ocean are shown that have the same properties as Figure 3. A report by Millard (1968) is cited that also show a similar spectrum.

The problem addressed in this study is to provide the best estimate of the horizontal vector wind for numerical forecasting purposes and for synoptic meteorological purposes. It is shown that the best that can be done is to give the wind, for a homogeneous area of flow, to within a

standard deviation of about one knot.

Equation 2 represents the simplest way to estimate a synoptic scale wind. It corresponds to the so-called "box-car" or rectangular weight function in which the limits of integration are set from $-\infty$ to $+\infty$ and a function $G(t - t_o)$ equal to $1/T$ for $t - T/2 < t_o < t + T/2$ is inserted after the integral sign. This weight function is not too good in its effect on the spectrum of the wind because it does not act like a sharp low pass filter. Frequencies both below $2\pi/T$ and above $2\pi/T$ are passed in varying amounts by the filter. A properly normalized weight function of the form $\cos \pi(t - t_o)/T$ can be shown to improve the filter characteristics, for example.

It is to be expected that improved ways to process anemometer data will result from further work in this problem area. For example, Baer and Withee (1972b), have studied how to locate and report the sudden changes, as a function of time, in wind direction and speed that occur during frontal passages.

For the purposes of this study of the aircraft program and of the results to be expected from S193, it should be noted first of all, that a scattering of data buoys over the ocean comparable to the scattering of ships in the results of Druyan(1971) could provide calibration points for a radar-radiometer system on a spacecraft in the form of properly averaged vector winds good to about 1 knot standard deviation in speed and a few degrees in direction.

It should also be noted that there is room for improvement in the area average indicated by equation (5). The average need not be restricted in concept to an average of weight one inside a certain area and zero outside the area. A properly chosen weight function can filter the wave number spectrum of the horizontal wind for numerical prediction purposes very efficiently.

Taylor's Hypothesis. - Taylor's hypothesis provides a means to relate measurements of the wind at a point as a function of time to measurements of the wind along a line (usually in the upwind downwind direction) as a function of distance. One way of describing the hypothesis is to say that it assumes that the pattern of turbulence is "frozen" and is advected past a point by the mean wind. This is equivalent to the assumption that the length of an eddy in space is given by multiplying the period of an eddy in time by the mean wind speed.

Lumley and Panofsky (1964) state that "Lappe, Davidson and Notess (1959) show by a comparison between tower measurements and airplane measurements at 90 and 120 m high, respectively, (the higher speed airplane measurements are almost sure to be satisfactory) that the hypothesis appears to be valid for horizontal wind fluctuation but that the vertical fluctuation measured by airplanes contains more low-frequency energy than the tower measurements. The authors ascribe this discrepancy to the effect of wind shear described by Lin. On the other hand, however, the terrain is not homogeneous, and flow patterns fixed relative to the ground contributing to the airplane, but not to tower measurements, may be responsible for the discrepancy".

"In summary, the very limited information seems to indicate that Taylor's hypothesis is generally applicable except for the low wave number components of vertical velocity fluctuations. Therefore all time spectra and correlation functions observed at a fixed point or from airplanes will, in what follows, be interpreted as space spectra and correlation functions along the direction of mean motion".

More recently, multiple arrays of wind sensors seem to suggest that eddies are dispersive. Typically, eddies can travel about six times their own length before they die out as shown by McDonald and Herrin (1971). The use of the Taylor's hypothesis in what follows is conservative. The additional decorrelation that is observed would increase the estimates of the number of degrees of freedom.

Argus Island Anemometer Data. - Figure 4 shows a small segment of an anemometer record obtained at Argus Island during Mission 119 (1970). This particular segment is a portion of the record obtained during the time near Flight 7, Run 1, Line 1. It shows the winds fluctuating from 12 knots to 21 knots in 60 seconds. A total of 2000 values of this Argus Island anemometer record were read every 4 seconds 1000 values before the Flight 7, Run 1, Line 1 measurements and for 1000 values after.

The covariance function for the anemometer record is shown in Figure 5. The variance spectrum is shown in Figure 6 as plotted on a relative scale. The covariance function shows a quasi-exponential non-oscillatory decay out to 144 seconds as plotted. At 400 seconds, the covariance is still equal to 0.28 or about 7% of the value at the origin.

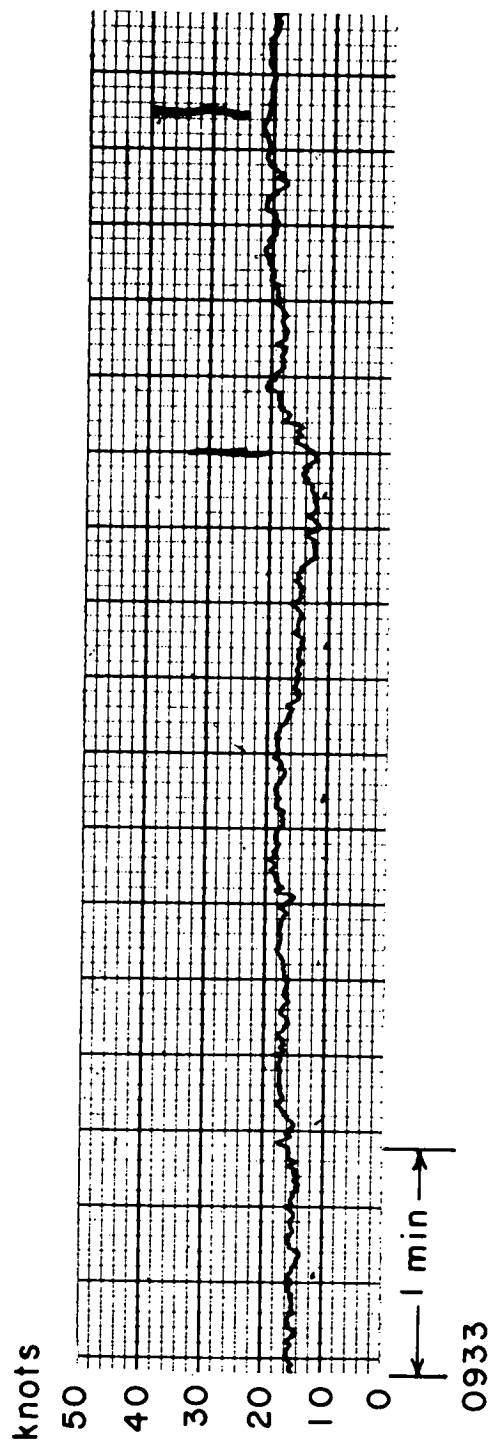

ARGUS ISLAND WIND RECORD

FIG. 4

Each spectral estimate has about 40 degrees of freedom according to Blackman and Tukey (1958). The spectrum shows that the major portion of the variability is concentrated in the low frequencies, corresponding to periods of 50 seconds and higher.

A well-known problem in statistics, is that of estimating the mean and variance of a normal population given a sample of N independent observations from a given population and of determining the variance and standard deviation of the estimate of the mean. For a sample of N independent observations the variance of the sample mean is given by the estimate of the variance $(SD_v)^2$ of the population divided by N as in equation 6.

$$\sigma^2_{\bar{V}} = \frac{(SD_v)^2}{N} \tag{6}$$

The 2000 points in the anemometer record are not independent and therefore equation 6 cannot be used with N equal to 2000. There are several ways to account for the correlation between points in such a time series. An equation given in Neumann and Pierson (1966) as given originally in Blackman and Tukey (1958) accounts for the decorrelations at different lags and provides for an effective number of degrees of freedom N^* as in

$$N^* = \frac{N}{m} \frac{[\Sigma S^*]^2}{\Sigma (S^*)^2} \tag{7}$$

where m is the number of smoothed spectral estimates available and the S* are the hanned spectral estimates. This equation holds best for spectra that do not depart too much from a white noise spectrum.

For this particular anemometer record, the effective number of degrees of freedom may be only about 178. The 2000 point autocorrelated record is perhaps the equivalent of a totally uncorrelated sample of 178 values from a normal population. The standard deviation of the sample mean is thus quite a bit larger than it would be for the same variance if the sample had consisted of 2000 independent points.

If the 178 independent points were thought to be equally spaced over the 2000 point time history, they would be located at about every 11th point, or every 44 seconds. This statement needs to be interpreted properly. Clearly from Figure 5 the covariance is still fairly high at

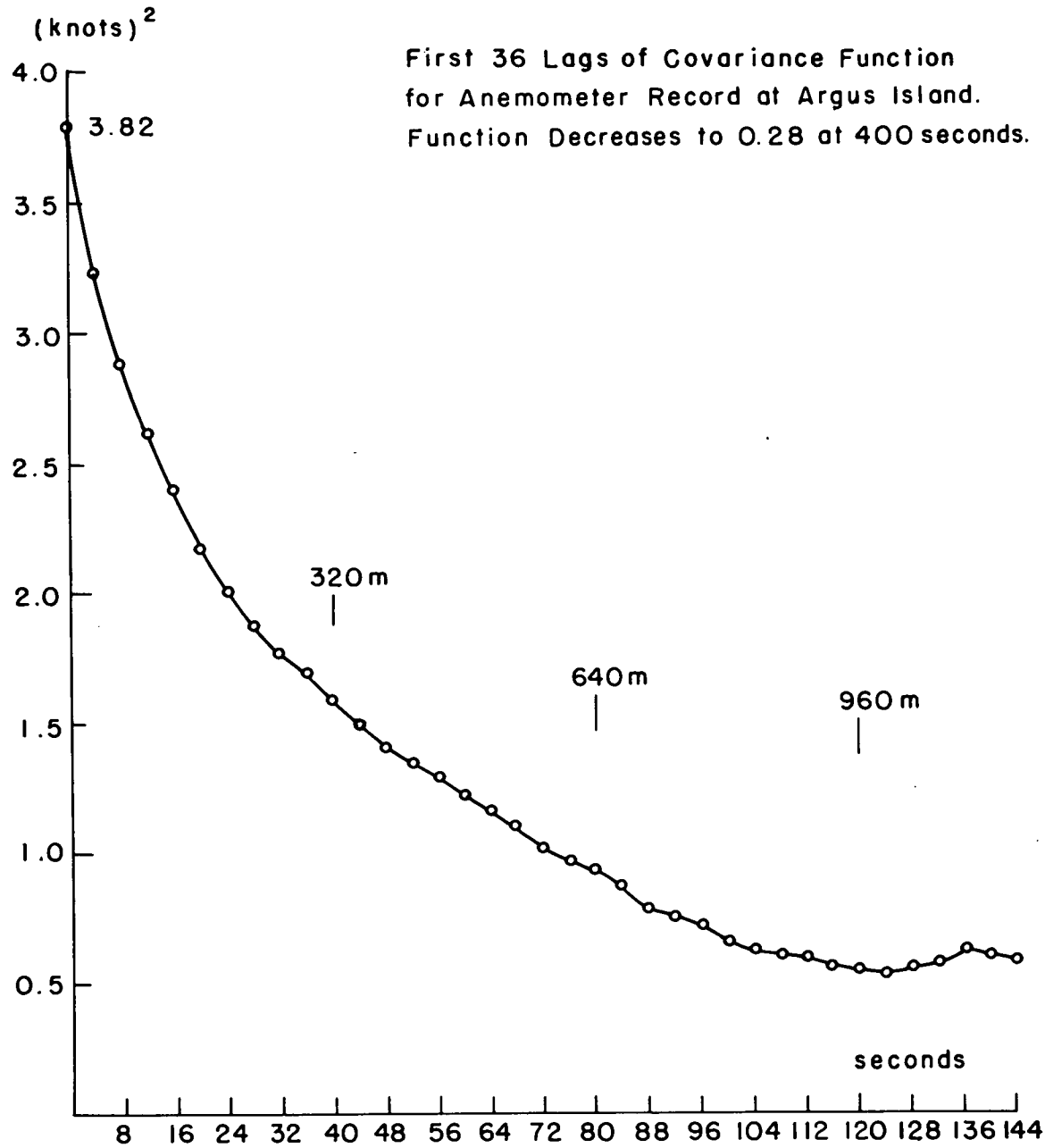
(knots)²
First 36 Lags of Covariance Function
for Anemometer Record at Argus Island.
Function Decreases to 0.28 at 400 seconds.
4.0
3.82
3.5
3.0
2.5
2.0
1.5
1.0
0.5
320m
640m
960m
seconds
8 16 24 32 40 48 56 64 72 80 88 96 104 112 120 128 136 144

FIG. 5

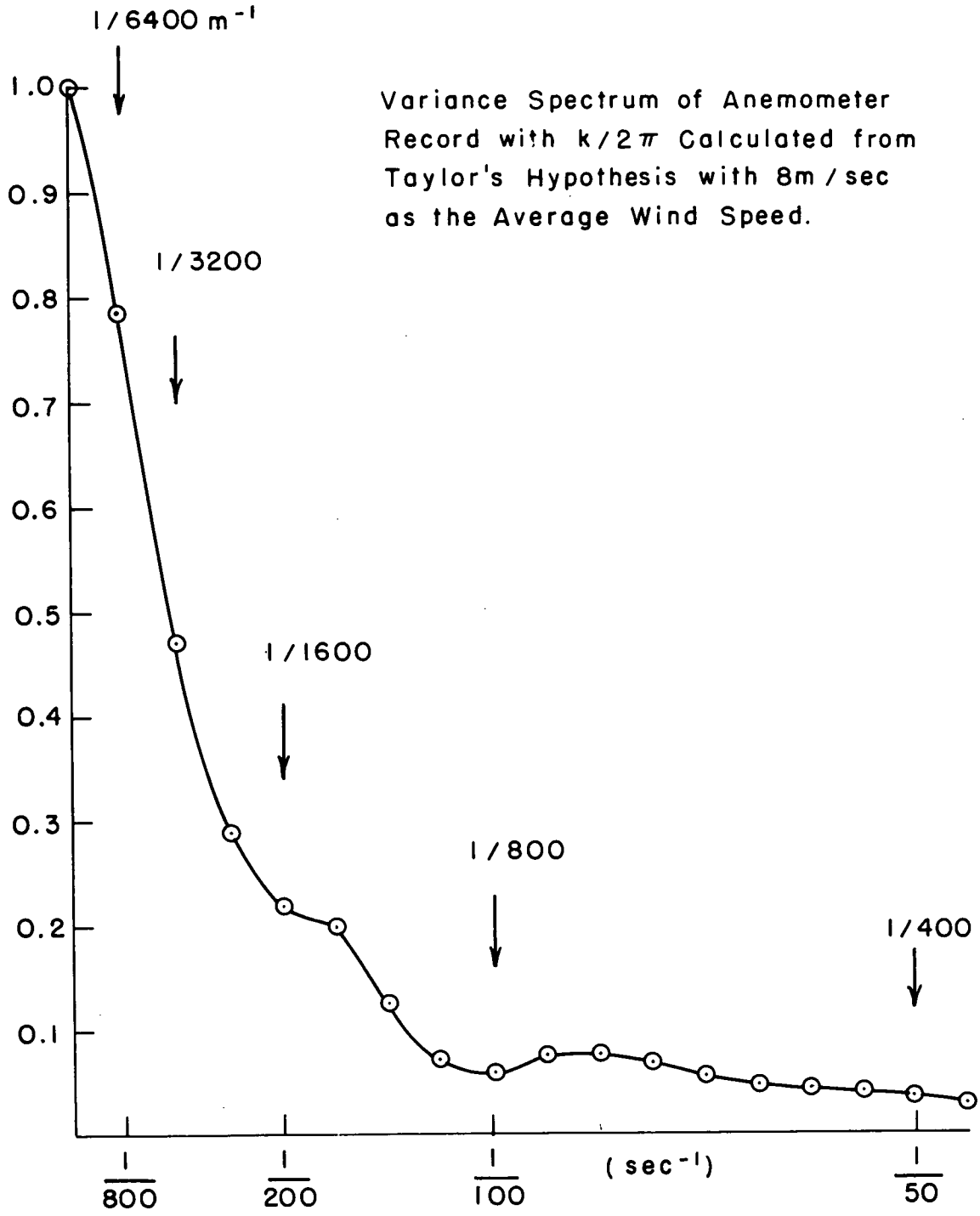
1/6400 m⁻¹
1.0
0.9
1/3200
0.8
0.7
0.6
0.5
1/1600
0.4
0.3
1/800
0.2
1/400
0.1
Variance Spectrum of Anemometer Record with k/2π Calculated from Taylor's Hypothesis with 8m/sec as the Average Wind Speed.
1/800
1/200
1/100
(sec⁻¹)
1/50

FIG. 6

44 seconds. The real point is that this complicated, non-independent time series of points contains enough information on the variance of the process and its frequency content to make it possible to replace it by an equivalent N^* independent points for the purpose of determining confidence intervals on $\overline{V}$. The 44 second apart effectively independent points in the anemometer record, if advected at a speed of 8 meters per second, implies that points 350 meters apart along an upwind line in space would be effectively independent in this same sense.

General Properties of the Turbulent Wind. - It is just as difficult to get a reliable estimate of the mean wind when a radar measurement is made over the ocean as it is to get a reliable estimate of the radar scattering cross section. In the plots and tables to follow, the scatter is caused just as much by inadequacies in the wind speed measurements as it is caused by the possible errors in the radar measurements.

In working with the turbulent wind, meteorologists study both the spectra and cross spectra of the $\vec{V}'$ components as described above and the vertical velocity fluctuations, w'. They also study the variation of the mean wind as a function of elevation above the ocean surface, $\vec{V}(z)$.

The variation of mean wind with height above the ocean surface depends on the stability of the layer of air over the water, which in turn is controlled by the air-sea temperature difference. If the air-sea temperature difference is small, the lapse rate in the atmosphere is adiabatic and the wind varies with height according a logarithmic wind profile. If the air is colder than the water the atmosphere is unstable, and, for the same wind above the surface there will be a greater stress on the surface. Conversely, with the air warmer than the water the atmosphere is stable and for a given wind above the surface, it will be less.

All of these factors were taken into account by Cardone (1969) in developing a computer based procedure for studying the winds in the planetary boundary layer. They are also taken into account in the interpretation of the winds for the various missions. The winds reported and used in these studies are the "equivalent" winds for a neutrally stratified atmosphere referred to 19.5 meters above the ocean surface. They would produce the same stress at the surface as the measured wind at some other elevation with some known air sea temperature difference according to the available theories on the subject. In general, the effect of air-sea temperature difference is relatively unimportant for high winds.

The fluctuations in wind speed recorded by a cup anemometer are more or less the equivalent of the fluctuations of the vector component of the wind in the direction of the mean wind. The spectrum shown in Figure 6 is typical of such spectra in that a record 8000 seconds long does not resolve the maximum away from the origin.

In general, according to Lumley and Panofsky (1964), the variance of this turbulent spectrum grows as the square of the mean wind as in equation 8

$$VAR = (SD_v)^2 = \int_0^\infty S(n)\, dn \cong K \overline{V}^2 \qquad (8)$$

when the wind is measured at a fixed height.

The value of SD_v is relatively constant with height so that, since the mean wind increases with height, the "relative gustiness" $SD_v/\overline{V}$ decreases with height. For a fixed height $SD_v/\overline{V}$ is also dependent on the air-sea temperature difference. In general, $SD_v/\overline{V}$ can be considered to range from about 0.10 to 0.30 with high values reserved for unstable air and light winds.

For the anemometer record being studied the mean wind was 17.0 knots before correction for height above the surface and stability effects and the standard deviation was 1.95 knots so that, at anemometer height,

$$\frac{SD_v}{\overline{V}} = 0.114 \qquad (9)$$

THE AIRCRAFT PROGRAM

Radar Sea Return Measurements and Wind Speed. - The scatterometer used to measure sea return was a continuous wave radar with a vertically polarized fan beam that differentiated the angle θ off the vertical by means of Doppler shifts in the backscattered radiation. Bradley (1971) has carried out an extensive analysis of this system. This study relies heavily upon his analysis, differing however, in some important points.

A typical upwind data run would be obtained by flying for about five minutes in a direction chosen visually to be perpendicular to the direction of the oncoming waves at the sea surface. The backscattered signal from ahead is upshifted in frequency, while that from behind is downshifted. Appropriate signal processing techniques yield measurements of σ^o in the vertical transmit vertical receive mode for various angles off the vertical.

The largest slice of recorded data that could be handled by the available computer at MSC was 0.3275 seconds long, and every fourth one of these data slices (spaced consequently 1.31 seconds apart) was chosen for analysis. Each 0.3275 second data slice yielded a measurement of σ^o at all desired angles. A four minute data run would yield about 180 separate measurements of σ^o for each angle. For such a run, a single average value of σ^o obtained from the individual values computed from each 0.3275 second sample was obtained for comparison with the average measured, or estimated, wind speed. Data processed for the different runs varied in duration, so the number 180 is appropriate only for a 4 minute run.

Bradley (1971) has given the result of a regression analysis of σ^o on $\overline{V}$ for the data obtained during Missions 119 and 156.

The values of A and B in equation (10) were determined for upwind and cross wind conditions for 35°, 25°, and 15° as a least square regression of log $\overline{V}$ on $\overline{\sigma}^o_N$. The values of A and B are given in Table 1.

$$10 \log_{10} \frac{\overline{\sigma}^o(\theta)}{\overline{\sigma}^o(10°)} = A + B \log_{10} \overline{V} \qquad (10)$$

TABLE I.- RESULTS OF CURVE FITTING BY BRADLEY (1971) FOR MISSIONS 119 AND 156

Wind Direction	θ	A	B	RMS Error
upwind	15°	- 7.51	3.30	0.717 db
	25°	-25.56	11.21	0.892
	35°	-34.42	14.93	0.882
crosswind	15°	- 6.68	2.13	0.748
	25°	-22.84	7.51	1.196
	35°	-35.51	12.62	1.355

The use of equation 10 to study the individual values of σ^o provides a great amount of information on the nature of the return. Denote $\overline{\sigma}^o(\theta)/\overline{\sigma}^o(10°)$ by $\overline{\sigma}^o_N(\theta)$ in equation 10 so that

$$10 \log_{10} (\overline{\sigma}^o_N(\theta)) = A + B \log_{10} \overline{V} \qquad (11)$$

A change of $\Delta\sigma^o_N$ in $\overline{\sigma}^o_N$ must produce a corresponding change of ΔV in V as in equation 12.

$$10 \log_{10} (\overline{\sigma}^o_N + \Delta\sigma^o_N) = A + B \log_{10} (\overline{V} + \Delta V)$$

$$= A + B \log_{10} \overline{V} + B \log_{10} \left(1 + \frac{\Delta V}{\overline{V}}\right) \qquad (12)$$

If equation 11 is subtracted from equation 12, the result is equation 13.

$$1 + \frac{\Delta\sigma^o_N}{\sigma^o_N} = \left(1 + \frac{\Delta V}{V}\right)^{B/10} \qquad (13)$$

Changes in $\Delta\sigma^o_N$ (one of the individual values observed as a time series during a particular flight line) are caused by two effects: (1) the radar backscatter is a random variable because of the noiselike character of the fading and (2) the backscattered signal strength changes because of actual changes in the roughness of the surface.

The variability of the measurements of σ^o due to fading depends on the total number of independent samples in the return signal. Bradley (1971) has given the formula for this source of variability and from it, it is possible to compute SD_σ, the standard deviation of σ^o_N.

From equation 13, $1 + \Delta V/\overline{V}$ and $1 - \Delta V/\overline{V}$ can then be computed as in Table II.

TABLE II. - VARIATION OF APPARENT WIND SPEED DUE TO FADING FOR A 0.3275 SECOND MEASUREMENT FOR AN UNDERLYING SURFACE WITH CONSTANT ROUGHNESS.

θ	$1 + \frac{\Delta\sigma^o_N}{\sigma_N}$	$1 + \frac{\Delta V}{V}$	$1 - \frac{\Delta V}{V}$
15°	1.12	1.41	0.71
25°	1.13	1.12	0.89
35°	1.15	1.10	0.91

The equivalent values in db for $1 + \Delta\bar{\sigma}^o_N / \bar{\sigma}_N$ in Table II are 0.49, 0.53 and 0.62 db.

Fading for this particular instrument over a uniformly rough surface amounting to 12% thus causes 41% apparent wind fluctuations at θ equal to 15°. At 35°, in contrast, fading produces only 10% apparent fluctuations in the wind. For example, if the true wind had been 30 knots, a value of σ^o at 15° could have been obtained that would indicate a wind as high as 42 knots or as low as 21 knots for about one-third of the values. At 35°, the wind could be computed to be as high as 33 knots and as low as 27 knots.

The scattering cross section will also vary if the roughness of the underlying surface varies. This roughness is dominantly controlled by the capillary wave structure, and as shown in Figure 1, the roughness increases with increasing wind speed. The capillary waves respond very quickly to variations in the wind speed so that if the wind is, say, 20% higher than the mean over a particular illuminated cell, σ^o will increase accordingly. The amount of this change is shown in Table III. Possible values for the ratio of the standard deviation of the wind speed to the mean wind speed are listed across the top of the table. The body of the table contains the resulting change of $1 + \Delta\bar{\sigma}^o_N / \bar{\sigma}_N$ and the equivalent value in db.

TABLE III. - VARIATION OF $1 + \Delta\sigma^o/\sigma^o$ IN TERMS OF FLUCTUATIONS OF THE WIND ABOUT THE MEAN WIND SPEED AS EXPRESSED BY $SD_v/\bar{V}$

	$SD_v/\bar{V}$ = 0.15		0.20		0.30	
	$1+\Delta\bar{\sigma}^o/\bar{\sigma}^o$	db	$1+\Delta\bar{\sigma}^o/\bar{\sigma}^o$	db	$1+\Delta\bar{\sigma}^o/\bar{\sigma}^o$	
15°	1.05	0.20	1.06	0.26	1.09	0.38
25°	1.18	0.73	1.23	0.89	1.34	1.28
35°	1.23	0.91	1.31	1.18	1.48	1.70

For example, if $SD_v/\bar{V}$ is 0.20 and the mean wind is say 30 knots, there will be patches over the ocean where the wind gusts will be 36 knots, and at 35°, σ^o would increase by 1.18 db if the average value of σ^o for a 36 knot wind were recorded.

Of course, these two effects occur together. A high gust will produce sea return that scatters about the expected value for that high wind according to the values in Table II. For example, a 30 knot average wind could have a local gust of 36 knots where the expected sea return would be 1.18 db higher because of the gust. However, sampling variability due to fading would produce fluctuations of ± 0.62 db about this value.

It is important to note that the fading effect is large for small θ and small for large θ whereas the variation in wind speed produces a large effect for large θ and a small effect for small θ.

For future study, the bar over $\bar{\sigma}^o(\theta)$ and over V can be removed and equation 10 can be written as equation 14.

$$10 \log_{10} \frac{\sigma^o(\theta)}{\bar{\sigma}^o(10°)} = A + B \log_{10} V$$

$$= 10 \log_{10} a + B \log_{10} V \quad (14)$$

Now, for example $\sigma^o(\theta)$ represents the individual values determined by 0.3275 second averages obtained every 1.31 seconds during an upwind flight at, say, 35° and V represents the wind speed that would be computed by solving for V in equation 14 as in equation 15.

$$V(\sigma^o(\theta)) = 10^{\frac{10}{B}\log_{10}\frac{\sigma^o(\theta)}{a\,\bar{\sigma}(10°)}} = \left[\frac{1}{a}\frac{\sigma^o(\theta)}{\bar{\sigma}(10°)}\right]^{\frac{10}{B}} \qquad (15)$$

Segments of the graphs that result from treating the successive values of σ^o as a time series and computing $V(\sigma^o(\theta))$ for 35°, 25°, and 15° for Flight 7, Run 1, Line 1 (an upwind run) are shown in Figure 7.

The aircraft ground speed should be added to the mean wind speed to obtain the speed of the aircraft relative to the "frozen" field of turbulence. The measurements of σ^o, 1.31 seconds apart are effectively 127 meters apart in the turbulence pattern. Were the pattern advected by the mean wind at, say, 8 meters per second, equivalent measurements by an anemometer would be about 16 seconds apart. A four minute long aircraft flight is thus the equivalent of a $(16/1.31) \times 4 \cong 49$ minute anemometer record.

These three functions do not look very much like the anemometer record of the wind shown in Figure 4. The one for 35° looks the most like an anemometer record, and the one for 15° has fluctuations in it for an excess of what could be expected in an anemometer record.

The analysis of these three space histories (after the use of Taylor's hypothesis) is shown in the next six figures. Figures 8 and 9 show the covariance function and the spectrum for $V(\sigma^o(35°))$. Figures 10 and 11 show these functions for 25°, and Figures 12 and 13, for 15°. The spectral estimates as computed from formulas given by Blackman and Tukey (1958) have only seven degrees of freedom so that the confidence intervals are quite broad as shown in the figures.

The curves for 35° show that this record has a standard deviation of 2.75 knots and therefore a variance of 7.56 $(\text{knots})^2$. The covariance function in Figure 8 drops off to about one-half the value at zero at the first lag. It does not really get to zero until just short of 1 kilometer. The spectrum has a large contribution to the total variance in the wave number range below $1/2036\ m^{-1}$ and substantial contributions on to $1/508\ m^{-1}$.

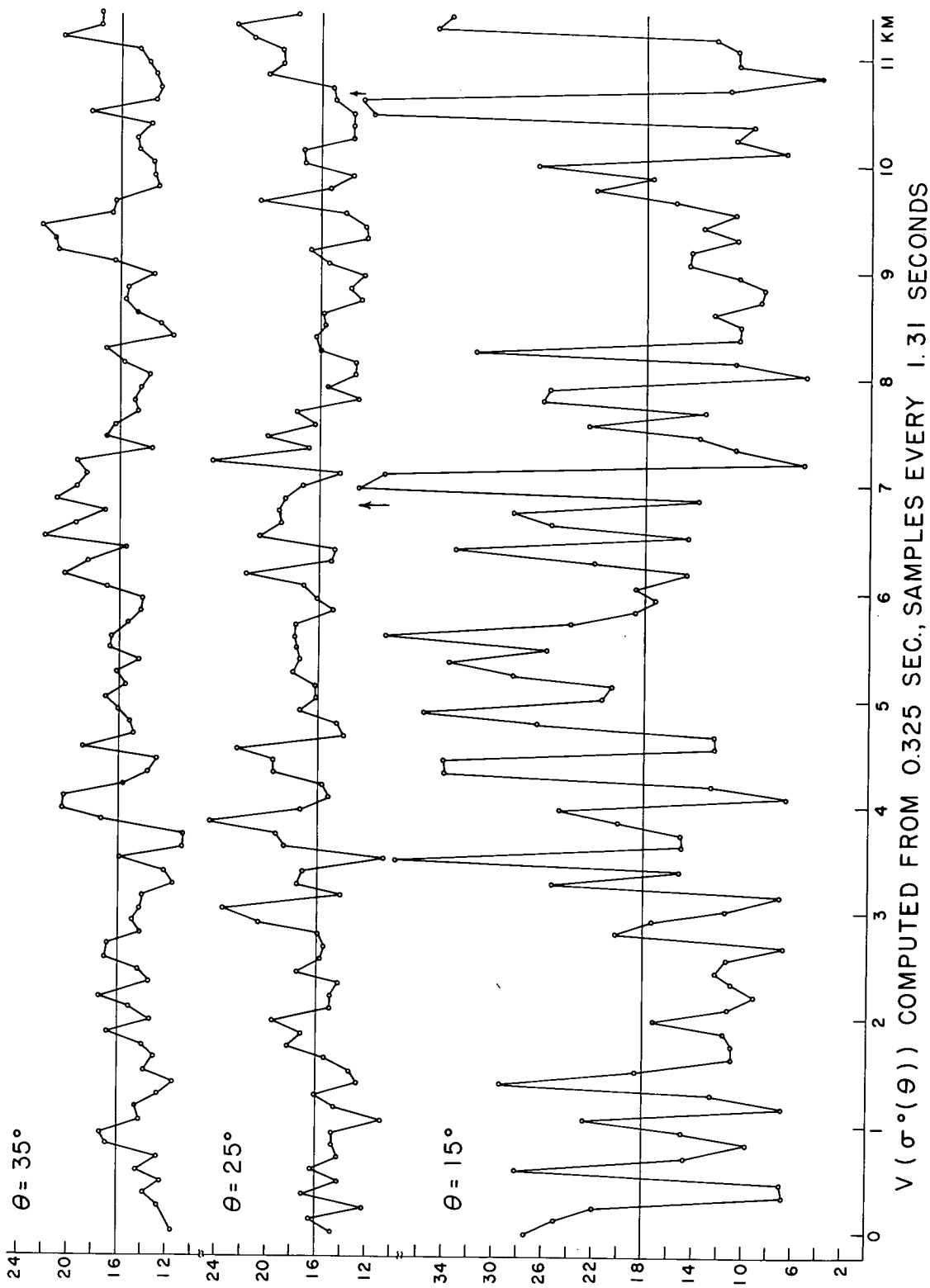

V (σ°(θ)) COMPUTED FROM 0.325 SEC., SAMPLES EVERY 1.31 SECONDS
FIG. 7

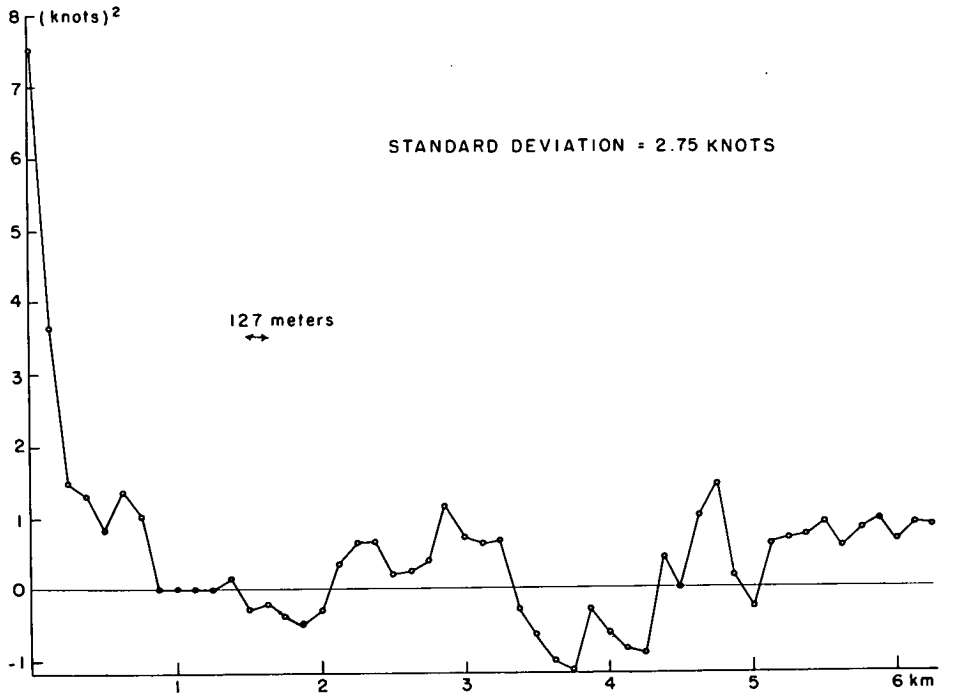

FIG. 8 COVARIANCE FUNCTION V [$\sigma°(35°)$]

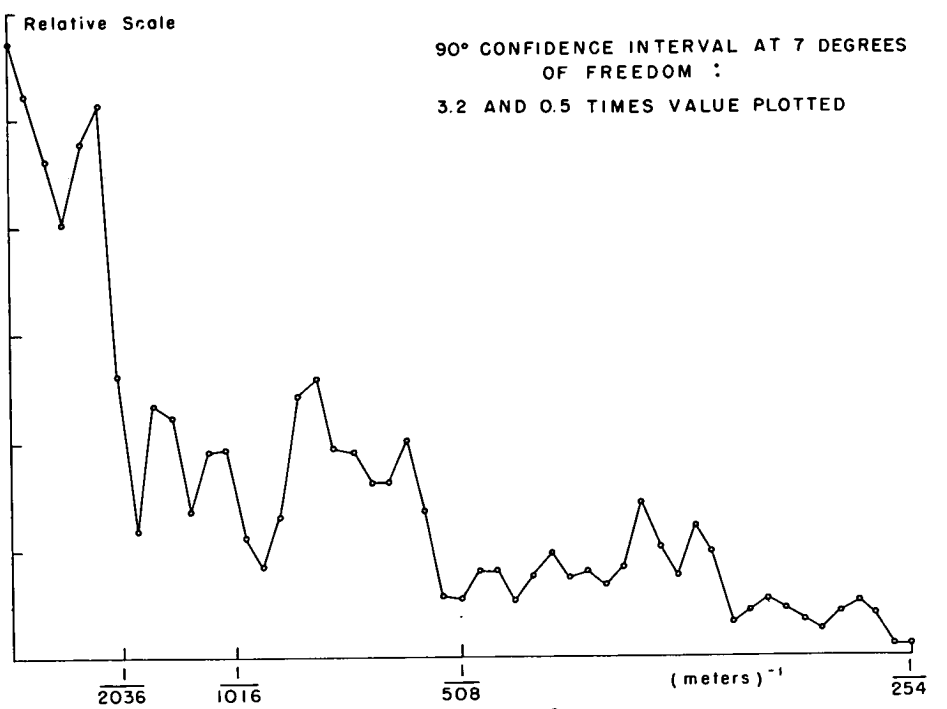

FIG. 9 $S(k/2\pi)$ for $\theta = 35°$

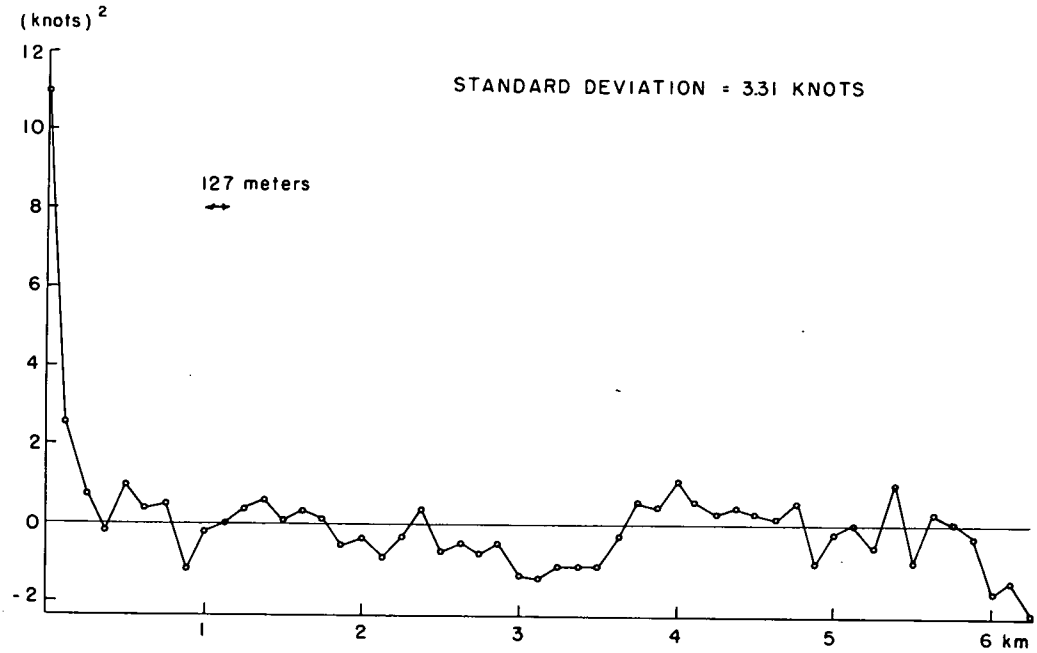

FIG. 10 COVARIANCE FUNCTION V [$\sigma°(25°)$]

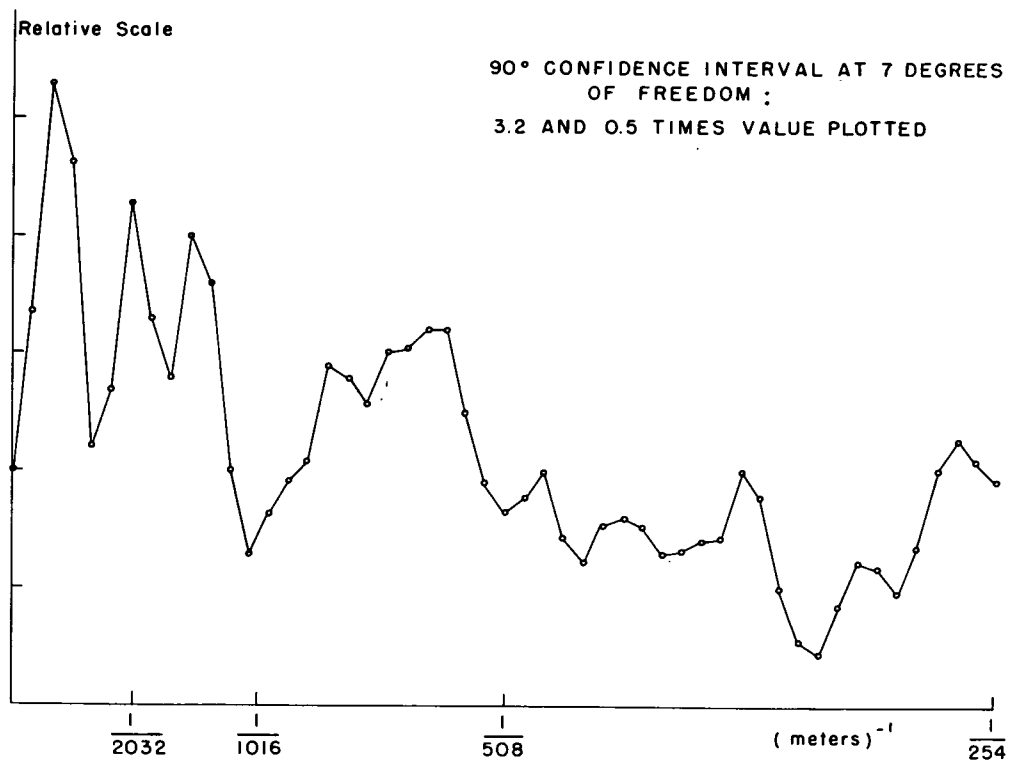

FIG. 11 S (k / 2π) for $\theta = 25°$

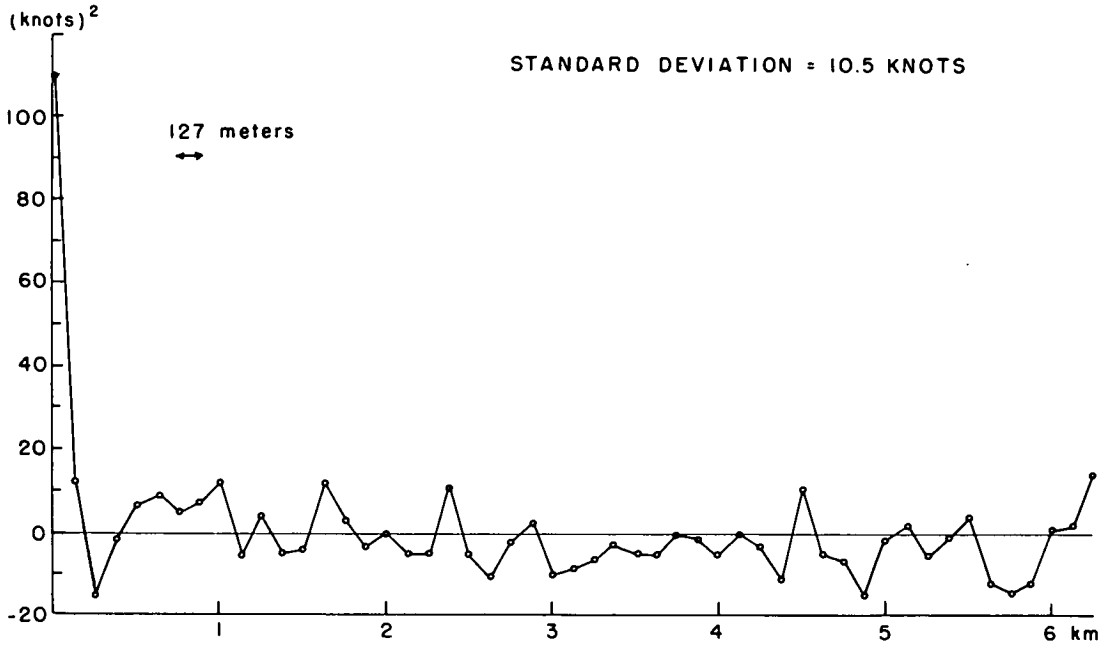

FIG. 12 COVARIANCE FUNCTION V [σ°(15°)]

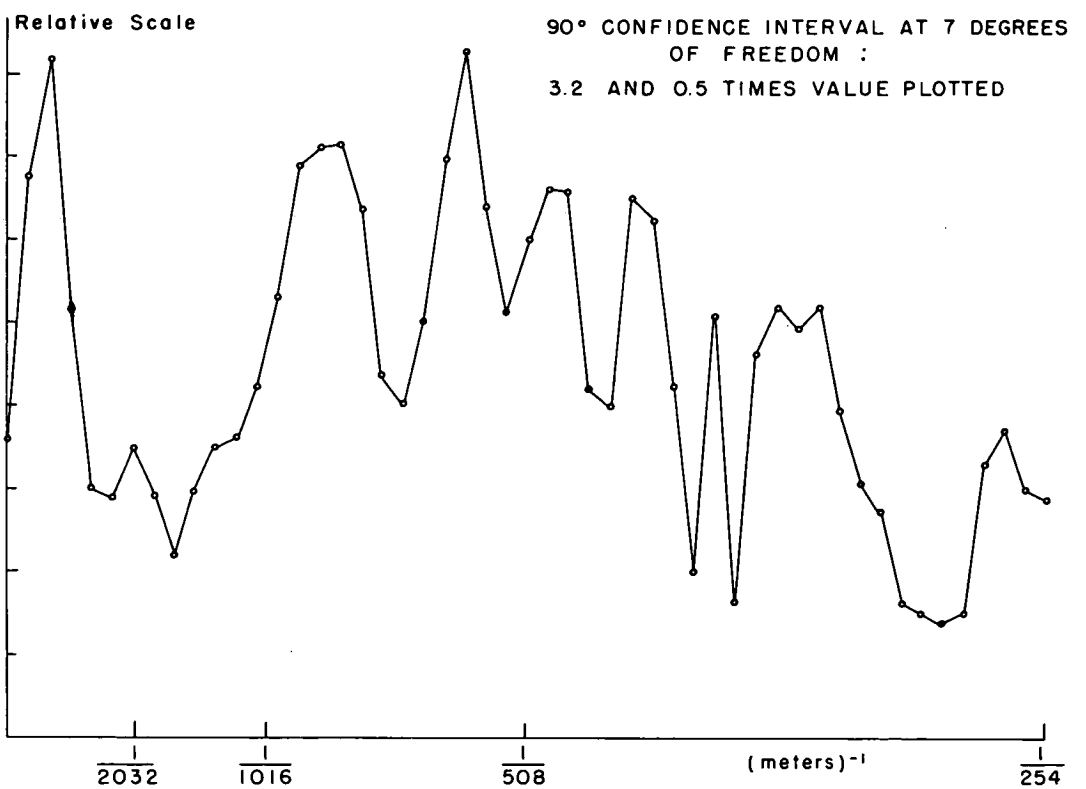

FIG. 13 $S(k/2\pi)$ for $\theta = 15°$

Figures 8 and 9 should be compared with Figures 5 and 6 from the anemometer record. The variance of the anemometer record was 3.82 (knots)^2, and the variance of $V(\sigma^o(35°))$ is 7.56 (knots)^2. The record graphed as $V(\sigma(35°))$ is thus a combination of the true fluctuations of the wind over the water and fading as described by Tables II and III. The peak at the left represents the anemometer fluctuations, which contribute 3.82 (knots)^2 to the variance, and the nearly flat part on the right, represents the superimposed white noise effect of the uncorrelated fading fluctuations which contribute 3.74 (knots)^2 to the variance. They happen to be approximately equal for this particular set of circumstances.

For 25°, the corresponding figures are Figures 10 and 11. The variance is 10.96 (knots)^2 so that 7.12 (knots)^2 are due to radar white noise effects (fading) and the rest to actual wind fluctuations. The relative peak in the spectrum at low frequencies despite the fact that almost 70% of the variability in the series is uncorrelated noise is notable.

For 15°, the corresponding figures are Figures 12 and 13. The variance is 110 (knots)^2 and less than 3% of the variability would be attributable to actual fluctuations in the wind over the water. The covariance function oscillates in a random way above and below zero, and the spectrum, since each point has only seven degrees of freedom is essentially a white noise spectrum.

The most important feature of the preceeding analysis is that the radar sea return has been shown to be responsive to one, two and three knot fluctuations about the average wind speed over distances of about 127 meters on the sea surface for large θ. The hypothesis that a large part of radar sea return is in practically instantaneous equilibrium with the local wind is substantiaed by this analysis. The result of the analysis of these three time (or space) series are perfectly predictable from Tables II and III. Wind variability is large enough to be at least as important as fading at 35°, whereas at 15°, fading completely submerges any wind variability.

These same time series techniques can also be applied to the series of original values of σ^o at 10°, 15°, 25° and 35°. The spectra and covariance functions are remarkably like the ones for the transformed wind speeds despite the exponential transformation. From these spectra by means of equation 7, the effective number of degrees of freedom in the sample of 189 values of σ^o can be found.

It now becomes possible to put one standard deviation confidence intervals on the estimates of the mean values of such quantities as

$$10 \log_{10} \frac{\bar{\sigma}^{o}(35°)}{\bar{\sigma}^{o}(10°)}$$

as given in Table IV. The effective number of independent points instead of being 189 has been reduced to the values shown, but the loss of degrees of freedom is much less than in the anemometer record in which 2000 data points were equivalent to 178 independent points. It has been assumed that $\sigma^{o}(10°)$ is independent of the other σ^{o} values so the variances have been added and the lowest applicable degrees of freedom has been used.

TABLE IV. - ANALYSIS OF FLIGHT 7, RUN 1, LINE 1.

				189 data points	
θ	$10 \log_{10} \bar{\sigma}^{o}$	SD_{σ} (db)	VAR	N^{*}	$\sqrt{N^{*}}$
10°	10.28	0.823	0.68	152	12
15°	9.100	0.807	0.65	143	12
25°	1.596	0.975	0.95	142	12
35°	-7.056	1.081	1.18	95	10
35°-10°	-17.34	1.36	1.86		
25°-10°	- 8.68	1.28	1.63		
15°-10°	- 1.18	1.15	1.33		

$$10 \log_{10} \left(\bar{\sigma}(35°) / \bar{\sigma}(10°) \right) = -17.34 \pm 0.136$$

$$10 \log_{10} \left(\bar{\sigma}(25°) / \bar{\sigma}(10°) \right) = -8.68 \pm 0.107$$

$$10 \log_{10} \left(\bar{\sigma}(15°) / \bar{\sigma}(10°) \right) = -1.18 \pm 0.096$$

The normalized average σ_{N}^{o} values for 35°, 25°, and 15° have been estimated to within ± 0.136, ± 0.107, and ± 0.096 db respectively.

It will be recalled that the mean of the anemometer record was

17 knots the standard deviation was 1.95 knots. The degrees of freedom were estimated by one procedure to be 178 for an 8000 second (133 minute) record. The flight line was shown to be the equivalent of a 49 minute anemometer record so that the sampling variability in the estimate of the mean would have (49/133) × 178, or about 65 degrees of freedom. This results in an estimate of the one standard deviation confidence interval on the mean wind of $\bar{v} = 17 \pm 0.24$ knots.

This estimate of the variability of the mean wind is suspect because of the shape of the wind spectrum. It was checked by a further study of the anemometer record at Argus Island. Actual 49 minute overlapping samples of three portions of the record were averaged for times near Flights 9 and 7. The actual standard deviations of these averages were 0.33 knots, 0.38 knots and 0.55 knots. The range in the averages was 1.24 knots, 1.41 knots and 2.25 knots. The values of 0.38 knots and 1.41 knots apply to Flight 7, Line 1, Run 1.

Similar results have been given by Bradley (1971) for other data runs as well as this one. The method he used to estimate the standard deviation of the sample mean of σ^o was more conservative so that broader confidence intervals were obtained. The estimated variability of the winds is comparable. Nevertheless, even these confidence intervals are quite narrow.

All of these results have to be corrected for atmospheric stability and the elevation of the anemometer and for variations in the antenna pattern both within missions and from one mission to another.

For $\theta = 35°$, the results are summarized for most of the data obtained on Missions 119 and 156, after all appropriate corrections, in Table V. There are 20 data sets identified by flight and mission. The meteorologist's estimate of the wind is given by V_M, good to ± 0.5 knots. The value of σ_N^o is also given along with the wind computed from this radar measurement, V_R, as tabulated. The difference to one-tenth of a knot is also tabulated, and the root mean square value of the difference in 2.6 knots.

A scatter plot of V_R versus V_M is shown in Figure 14. The scatter is really not very large and is due to both the difficulties of specifying the wind from the meteorological point of view and the scattering cross section from a radar point of view.

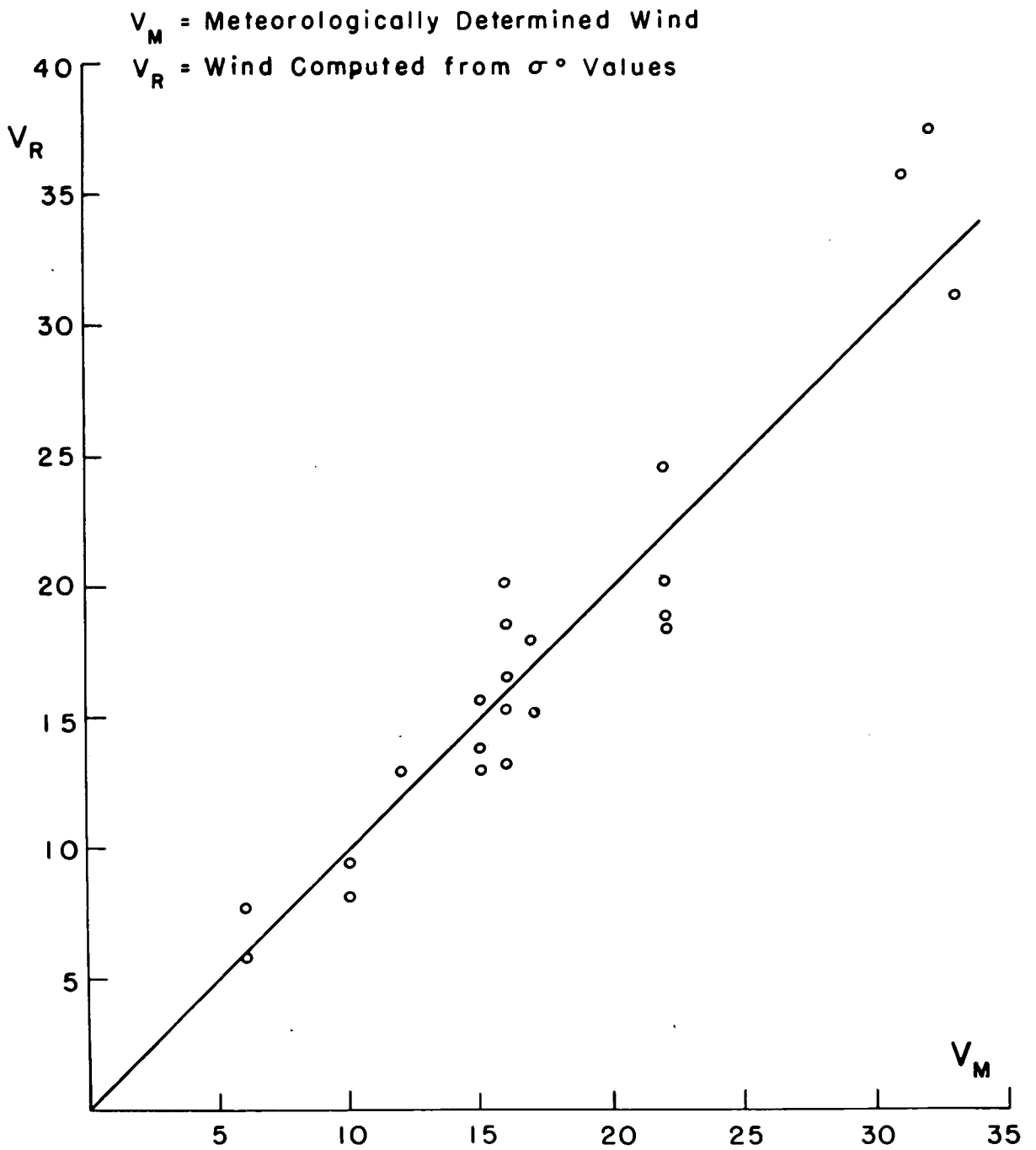

FIG. 14. SCATTER DIAGRAM OF WIND SPEED DETERMINED METEOROLOGICALLY VERSUS WIND SPEED DETERMINED BY RADAR.

TABLE V.- METEOROLOGICAL WIND ESTIMATES, σ^o VALUES AND WIND SPEED COMPUTED FROM σ^o VALUES FOR UP-WIND 35° INCIDENCE ANGLE FOR DATA FROM MISSIONS 119 AND 156.

Set	Mission	Flight	V_M	$\bar{\sigma}^o$(db)	V_R	Differences
1	119	9-3-3	6	-23.17	5.7	0.3
2	119	9-2-2*	6	-21.23	7.6	-1.6
3	156	3-4-5	10	-20.02	9.2	0.8
4	156	3-4-6*	10	-21.04	7.9	2.1
5	119	5-1-2	12	-18.02	12.6	-0.6
6	156	5-4-5	15	-16.65	15.5	-0.5
7	156	5-4-6*	15	-17.47	13.7	1.3
8	119	7-1-1	16	-16.25	16.5	-0.5
9	119	7-1-2*	16	-15.01	20.0	4
10	119	9-1-1	16	-16.88	15.0	1
11	119	9-1-2*	16	-15.5	18.5	-2.5
12	119	7-1-7	17	-15.70	17.9	-0.9
13	119	9-1-3	17	-16.85	15.0	2
14	156	7-8-5	22	-13.67	24.5	-2.5
15	156	7-8-6	22	-14.97	20.0	2
16	119	2-1-1	22	-15.69	18.0	4
17	119	2-1-2*	22	-15.52	18.5	3.5
18	156	2-8-1	31	-11.23	35.7	-4.7
19	119	3-1-2*	32	-10.96	37.3	-5.3
20	119	3-1-1	33	-12.15	31.0	2
				RMS ERROR		2.6 knots

An Inconsistency. - The data on Flight 7-1-1 show that the scatter in the measurement of a particular average scattering cross section is small. The scatter in the measurement of the average wind is also small. Moreover, the data show that the measurements of σ^o are actually responding to the gusts and lulls in the wind over the ocean surface along the path scanned by the beam.

On the other hand, the data in Table V and Figure 14 show a much larger scatter between the sea return and the wind, or the wind computed from the sea return and the meteorological wind, than can be explained on the basis of measurements made on a particular flight line

and run. Even if these estimates are off so that $\overline{\sigma_o}$ scatters by ± 0.3 db and $\overline{V}$ by $\pm$ 1 knot, the scatter in the full data set is still too large.

The greater scatter in the total set of data with rms errors of 0.7 db and 2.6 knots, or so, must be explainable in terms of factors other than the duration of the flight line and the concurrent measurement of the wind, especially for the Argus Island, Mission 119 results. These sources of scatter can be instrumental and meteorological and, or, oceanographic.

For example, the starred values for the flights in Table V were obtained with the aircraft flying downwind looking upwind with the aft pointing beam. Many of these values go with a corresponding set of values with the aircraft flying upwind looking upwind with the forward pointing beam. These pairs of measurements were made within just a few minutes of each other. Although Bradley (1971) attempted to calibrate out fore beam-aft beam antenna pattern differences, these values suggest the possibility of a residual error in this effect.

In processing the scatterometry data, one important part of the calculation is the ground speed of the aircraft, which is used in determining the Doppler shift. This in turn is used to calculate the backscatter for each angle. A study of the determination of the ground speed for Mission 119 lead to the conclusion that the ground speed was not determined with complete accuracy. Revised values of the ground speed are given by Pierson and Cardone (1971). The use of an incorrect value for the ground speed has two effects. It shifts the measured value to a value of θ different from the one desired, and it gives a value that needs to be corrected for by a different angle in the antenna gain correction. The combined effect is rather difficult to account for fully, but it can surely introduce additional scatter.

Other sources of residual error can be meteorological and/or oceanographic. The form of the wind profile with height and the drag coefficient must be known to be able to compute the variation of wind with height and the friction velocity. The scatter in such a basic quantity as the drag coefficient has been documented for Argus Island observations by DeLeonibus (1971).

There is also the problem of the effect of the Argus Island Platform and supporting structure on the wind flow past the anemometer on the tower. This effect was studied by Thornthwaite et al (1965) at Argus Island and by Mollo-Christenson and Seesholtz (1967) for a similar,

but smaller tower in a wind tunnel. For a south wind, the speed measured by the anemometer could be 4 or 5% too high. However, not enough information is available to make corrections for tower effects for the variety of wind directions encountered during Mission 119. Hence, no correction for this effect was attempted. The variation of this effect with wind direction could easily account for another $\frac{1}{2}$ to 1 knot scatter in the estimate of the average wind.

There is one oceanographic source of scatter that has not been removed from the data. The high frequency part of the wave spectrum is in equilibrium with the local wind but the lower frequency gravity wave portion need not be in equilibrium, as a fully developed sea, with the wind. Preliminary models of radar sea return show a dependence of σ^o on the longer higher waves in the spectrum and the present relationship can eventually be corrected for this variation in more complicated systems by means of both theory and multiple regression techniques. At the present level of development of the theory of sea return this added refinement is probably premature.

It is our opinion that much of this scatter has to do with meteorological, aircraft and radar instrument difficulties. With scanning pencil beam radars such as the one built under the AAFE Radscat program and for S193 on Skylab, a good part of this scatter may not be present. Under the AAFE Langley Radscat program, plans are being made to minimize the problems of estimating the average wind.

To study this problem further, the two sources of variability identified in the preceding sections will be extrapolated to spacecraft altitudes for S193. The result will be predictions of the capabilities of S193 in clear air to determine the wind speed and direction over the oceans under the assumption that the scatter in the data will be caused by the combination of fading and a turbulent wind over the water.

EXTRAPOLATION TO S193

The two sources of scatter in the measurement of σ^o obtained with aircraft that were identified in this report have their counterpart for S193 and the effects of both fading and turbulence can be taken into account for measurements to be made by S193. Both of these effects result in a very small scatter in the measurements.

Skylab S193 Scanning Patterns. - Three typical orbit segments for Skylab during which S193 might be turned on are illustrated in Figure 15. The wind field near the surface of the ocean as deduced from ship reports is illustrated in Figure 16 and the cloud cover that was present is shown in Figure 17.

Orbit segment A in Figure 15 shows the cross-track non-contiguous scanning mode. The antenna points straight down and at angles of 15.6°, 29.4°, 40.1 and 48° off of the vertical at the spacecraft. Because of the curvature of the earth the appropriate θ values will be larger than these angles.

The illuminated areas shown by the open circles are not drawn to scale. They are larger as the angle increases. At each cell, six different measurements will be made; σ^o_{VV}, σ^o_{HH}, σ^o_{HV}, and σ^o_{VH} and the passive microwave temperature for two polarizations. The pass shown would obtain 870 separate measurements in about seven minutes.

Orbit segment B shows a northbound pass and orbit segment C shows a southbound pass on the non-contiguous forward scanning mode. Each black ellipse represents a series of six measurements at each of the five different angles at nearly the same place on the ocean surface for a total of 30 measurements.

Figure 16 shows a wind field analysis such as might occur during a Skylab pass. The various scanning modes would scan cells on the ocean surface in which the wind speed varied all the way from 5 knots, or so, to perhaps 50 or 70 knots, depending on the scanning mode and the exact location of the radar illuminated areas on the sea surface.

The "radar scatter" or "fading variability" of S193. - S193 measurements have a source of scatter analogous to the fading that results from the 0.3275 second averages in the aircraft data. Each of the four S193 radar measurements are averaged over about 0.6 seconds and the bandwidth of the system is such that the received power is measured to within 7% for each measurement. Thus within one standard deviation the radar scattering cross section is good to within 1 ± 0.07 of the expected value. In fact, the averaging time is a function of the antenna angle and has been chosen so that this value is an upper bound for all scan angles.

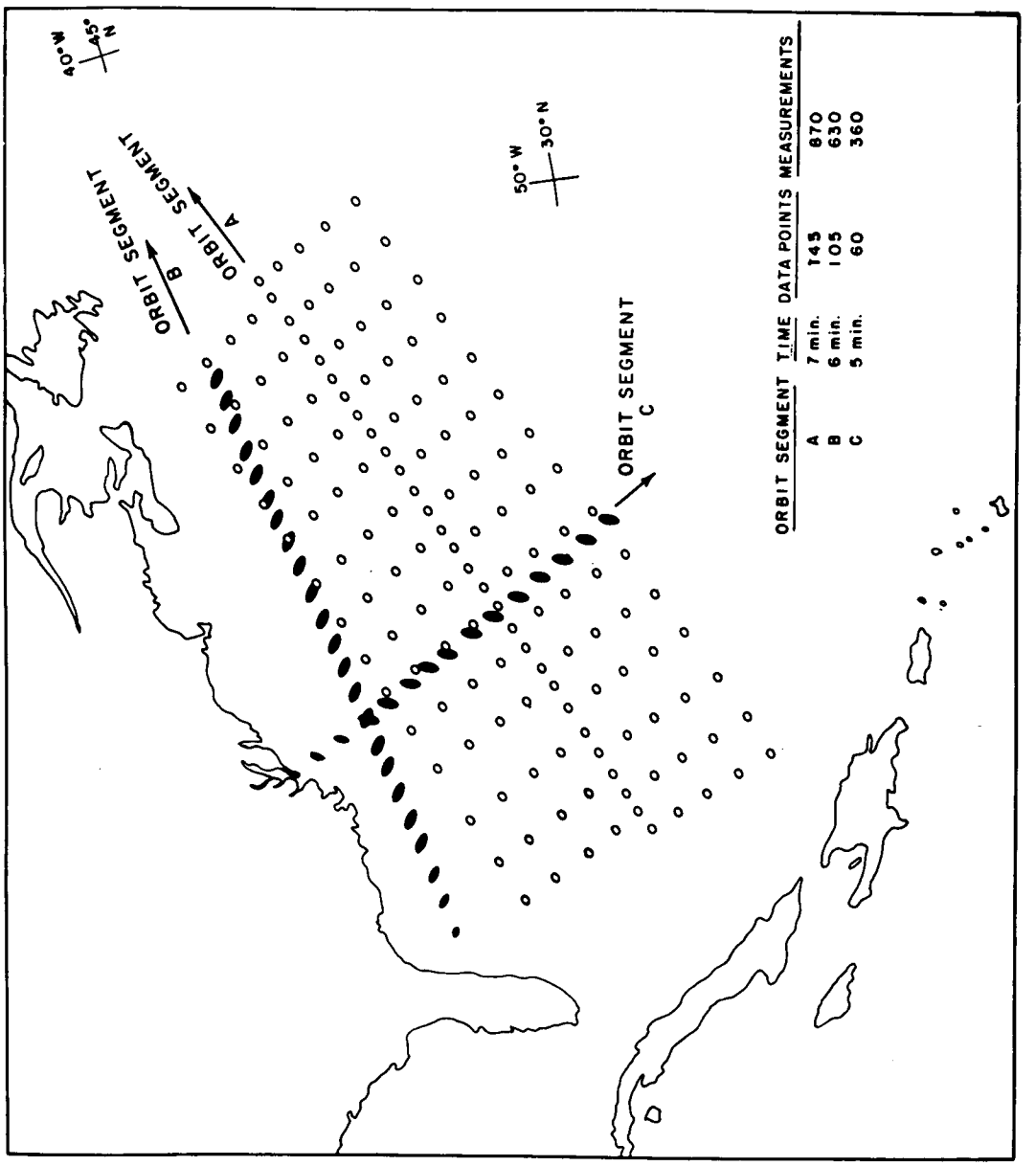

FIG. 15. CROSS TRACK AND ALONG TRACK SCANNING PATTERNS FOR S193 ON SKYLAB.

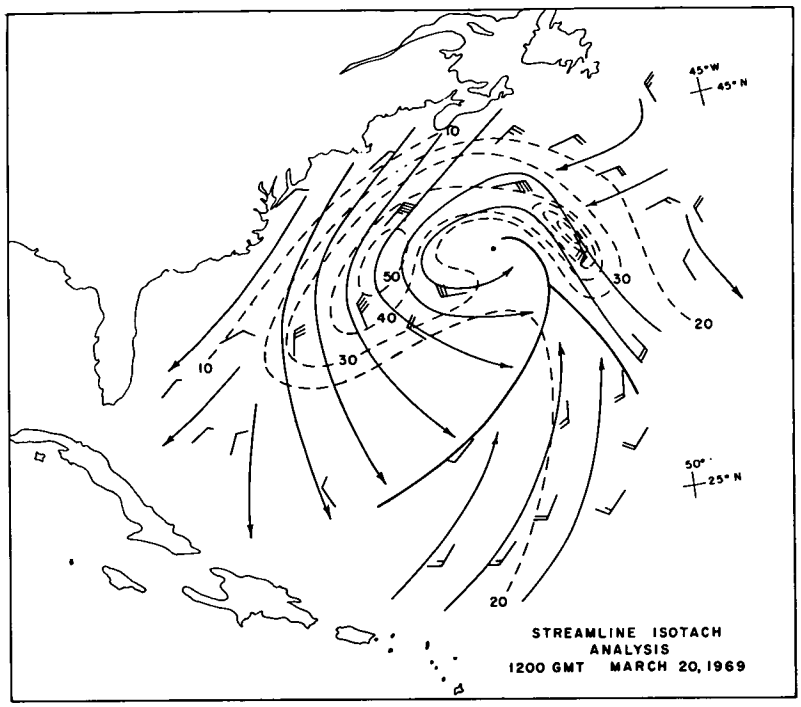
45°W
45°N
10
50
40
30
30
20
10
30
50°
25°N
20
STREAMLINE ISOTACH
ANALYSIS
1200 GMT MARCH 20, 1969

FIG. 16

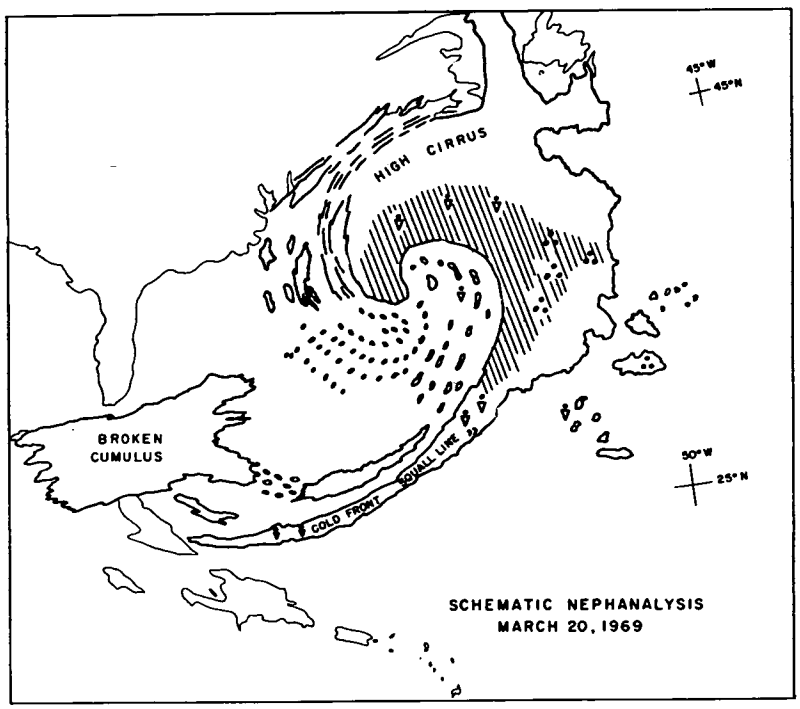
45°W
45°N
HIGH CIRRUS
BROKEN
CUMULUS
COLD FRONT
SQUALL LINE
50°W
25°N
SCHEMATIC NEPHANALYSIS
MARCH 20, 1969

FIG. 17

This design fact yields the standard deviation of measurements of σ^o which is $\pm$ 0.3 db. Table VI shows the results using this value for SD_σ in equation 13 for the off-vertical values of θ and the values of B found by Bradley (1971). The upwind B for 15° was used for 15.6°, the B for 25° was used for 29.4° and the B for 35° was used for both 40.1° and 48°. In actuality, the values for B for these angles are likely to be higher, which in turn implies a lower percentage variability in the wind estimates.

It also must be assumed that the same kind of equation as equation 11 will also be valid for non-normalized measurements of σ^o at these various values of θ. Since the transmitted power is monitored in S193, the values of σ^o should be primary measurements that will not have to be normalized to 10° as in the aircraft flights. The constant, A, will be different for the S193 measurements but the equation should still be of the same form. Results similar to Table VI can also be computed for cross wind conditions and somewhat larger percentages of scatter would result.

TABLE VI. - CONSERVATIVE ESTIMATES OF PER POINT VARIABILITY DUE TO FADING OF UPWIND WIND SPEED MEASUREMENTS BASED ON SINGLE MEASUREMENT OF σ^o BY S193.

$\log 1.07 = 0.030$	$SD_\sigma = 0.3$ db	
θ	$\log_{10}(1 + \Delta v/v)$	$1 + \Delta V/V$
15.6°	0.0909	1.23
29.4°	0.0266	1.06
40.1°	0.0201	1.05
48°	0.0201	1.05

In essence for angles of 29.4° and greater, the wind speed estimate for a single measurement of σ^o_{VV} will scatter by about $\pm$ 6% about the true value due to this source of variability. All theoretical and observational data to date suggest that σ^o_{HH}, σ^o_{HV} and σ^o_{VH} will all provide additional equally independent estimates of the wind-speed and that the scatter will be comparable. The average of four such estimates, since each one will be independent, will produce a final estimate within 3% of the expected value.

The available data on $\sigma^{o}_{VV}(\theta)$ as a function of wind speed all suggest that at $\theta = 0$, $\sigma^{o}_{VV}(0)$ decreases with increasing wind speed and that at an angle near 10°, or so, $\sigma^{o}_{VV}(\theta)$ does not depend strongly on wind speed. This is why the normalized measurements at 15° are relatively insensitive to wind speed and why the values for $1 + \Delta V/V$ and $1 - \Delta V/V$ are large for 15°. An operational instrument could avoid this problem by tilting the antenna forward as described by Moore and Pierson (1971). The values given for 15° in Tables I, II, III, IV, and VI are all a natural consequence of the shape of the scattering cross section curve and are therefore to be expected.

S193 also measures passive microwave temperature in two polarizations. Moore et al (1971) have combined the data obtained by Nordberg and Hollinger in a plot that shows that, given the sea surface temperature, ΔT_B(°K), increases at 0.96 ± 0.16 °K/(m/s) for 19 GHz as the wind varies from zero to 30 meters per second.

The variation of ΔT_{BHH}(°K) for 13.9 GHz will not be as strong as that at 19 GHz, but through cloudless skies after correction for atmospheric temperature and water vapor and without obvious corrections for fetch and duration, which change the amount of foam, a similar dependence about 75% as strong could lead to the dependence given by equation 16

$$V \cong (0.78 \pm 0.16)\, \Delta T_{BHH}(°K) \qquad (16)$$

It may then be possible to estimate the wind speed at 15° to within about 20% by a passive measurement. Refinements in calculating the amount of foam could reduce this scatter substantially. At 0°, there will again be a wind speed dependence for σ^{c}, which can be combined with the passive microwave to determine the wind.

Moreover, the passive microwave measurements appear to be independent of wind direction. It should be possible to devise a proceedure in which all six measurements for a θ greater than 15° can be used to determine both wind speed and direction to within a choice of four possible angles, $\pm X$ and $\pm X + 180°$, at each cell through cloudless skies. Three of these four angles can often be eliminated by synoptic considerations.

Effects of Turbulent Wind Field on Measurements Made with S193. - The patch of ocean illuminated by the radar beam on S193 varies in area and dimensions as a function of the angle of the beam off the vertical. The area of the patch is 95 km^2 for 0° and increases to 385 km^2 at 48° as shown in Table VII.

The area given in this table is computed on the assumption that the main lobe of the antenna pattern illuminates the sea surface with constant power over the entire given area and that there is zero power outside the area. It is also an instantaneous value. The time required to make the measurement spreads out the illuminated area and applies a trapezoidal weight function to a broadened pattern. This incremental area is also tabulated for the cross track mode, but it was not used in the rest of the calculations. This incremental area actually increases the value of N by an amount equivalent to adding about half the incremental area to the values tabulated under "area". The rest of the entries in the table are therefore conservative.

The analysis of the Argus Island anemometer record led to the conclusion that for a wind speed near 16 knots the anemometer record would be the equivalent of measurements of wind speed every 350 meters along a line on the ocean surface in the wind direction. Lumley and Panofsky (1964) show that the horizontal wind decorrelates in the cross wind direction at least as fast as in the upwind-downwind direction so that points on a square grid 350 meters on a side over the area illuminated by the radar beam could represent the equivalent number of independent observations of the wind. The wind at each of these points, and in fact over the entire area, is fluctuating above and below the desired average value as represented by equation 5 in much the same way that anemometer records fluctuate.

A square 350 meters on a side has an area of $(0.35)^2 = 0.123$ square kilometers so that there are effectively 8 independent points per square kilometer of illuminated area for a 16 knot wind.

The number of effectively independent points for a 16 knot wind is shown in Table VII for each antenna angle. These values have to be reduced by a factor of four when the wind speed is doubled and by a factor of nine when the wind is tripled because of the scaling laws for turbulence. Even for a 48 knot wind, there are at least 84 degrees of freedom in the vertical.

TABLE VII. - CONSERVATIVE DEGREES OF FREEDOM (N) IN ESTIMATES OF VARIANCE OF THE AVERAGE WIND OVER THE RADAR ILLUMINATED PATCH, AND 95% CONFIDENCE INTERVAL ON $\bar{V}$ FOR $SD_v/V = 0.20$ AS GIVEN BY $\bar{V} \pm (2SD_v/\sqrt{N})$.

Angle	0°	15.6°	29.4°	40.1°	48°
Area $(KM)^2$	95	108	151	236	385
Incremental Area $(KM)^2$	21	39	68	97	142
$N(\bar{V} = 16$ knots)	760	864	1208	1888	3080
$N(\bar{V} = 32$ knots)	190	216	302	472	770
$N(\bar{V} = 48$ knots)	84	96	134	209	347
$1/\sqrt{N}$ (16)	.036	.033	.028	.023	.018
$1/\sqrt{N}$ (32)	.072	.066	.056	.046	.036
$1/\sqrt{N}$ (48)	.109	.102	.086	.069	.054
95% Confidence Interval					
16 knots	16.24	16.20	16.18	16.14	16.11
	15.76	15.80	15.82	15.86	15.89
32 knots	32.92	32.85	32.72	32.59	32.46
	31.08	31.15	31.28	31.41	31.54
48 knots	50.09	49.96	49.65	49.32	49.03
	45.91	46.04	46.35	46.68	46.97

If the standard deviation of the wind is 20% of the mean wind, 95% confidence intervals on the mean wind can be found by computing as in Table VII.

These confidence intervals are delightfully narrow. For intercomparison with other numbers in this paper, they should be halved. The 95% confidence intervals are plus or minus less than 1 knot for all entries in the table except 48 knots. The largest percentage variation for 0° and a 48 knot wind is 4.4%. It can be concluded that the illuminated patch is large enough to provide a truly stable estimate of the average wind for the purposes of synoptic meteorology.

The dimensions of the spot illuminated by the radar beam are given in Table VIII. The spot at 48° is roughly elliptical with the doubled major axis distance equal to 29 km and the doubled minor axis distance equal to 17 km as an example from the table.

Here again the spot is actually stretched in one direction due to spacecraft motion. The stretching makes the values in the table conservative.

TABLE VIII. DIMENSIONS OF PATCH OF OCEAN ILLUMINATED BY S193 RADAR BEAM AND FREQUENCIES IN AN ANEMOMETER RECORD THAT CORRESPOND TO THESE DIMENSIONS.

Angle	0°	15.6°	29.4°	40.1°	48°
Area $(KM)^2$	95	108	151	236	385
Approximate Length (KM)	11	12	15	21	29
Approximate Width (KM)	11	12	13	15	17
Equivalent Time Minutes					
8 meters/sec	23	25	31	44	60
	23	25	27	31	35
16 meters/sec	11	12	15	22	30
	11	12	13	15	17
24 meters/sec	7	8	10	15	20
	7	8	9	10	12
Approximate Cycles/Hour					
8 meters/sec	2.6	2.4	1.9	1.4	1.0
	2.6	2.4	2.2	1.9	1.7
16 meters/sec	5.5	5.0	4.0	2.7	2.0
	5.5	5.0	4.6	4.0	3.5
24 meters/sec	8.6	7.5	6.0	4.0	3.0
	8.6	7.5	6.7	6.0	5.0

Consider a sinusoidal perturbation in the wind with a length in space given by these tabulated dimensions and assume that it is advected by the mean wind. Such a perturbation moving at 8 meters per second would take 60 minutes, as tabulated, to travel 29 km across the beam. The 29 km ocean distance is thus the equivalent of a perturbation with a period of 60 minutes in an anemomber record when the mean wind is 8 meters/sec.

The periods that result for each antenna angle and for the two distances across each patch are all given in Table VIII. They range from 7 minutes to 60 minutes. The reciprocals of these numbers converted to cycles per hour are given as the last set of entries. The values range from 1.0 to 8.6 cycles per hour. Either way, when these periods, or frequencies, are located on the spectrum in Figure 3, they all fall in the valley between the microscale turbulent fluctuations and the synoptic scale winds. The illuminated patch of sea surface from the scanning pencil beam on S193 acts as a very efficient way to obtain the quantity shown in equation 5 by acting as a low pass filter to suppress the microscale fluctuations and provide a very stable scattering cross section measurement representative of the desired synoptic scale wind.

The two dimensional "box-car", or square sided, weight function assumed for the antenna pattern is an over simplification of the problem. The power illuminating the surface decreases in a radial direction from some center spot whose location depends on geometry and the movement of the spacecraft during the time required for one measurement. To account for 96% of the total power involved, the dimensions of instantaneous pattern must be increased by a factor of 1.65 so that the area is increased by a factor of about 2.6. The exact form of the weight function will depend on many factors. It will, however, be a smoothly varying function that builds from zero to a unimodel peak, perhaps with roughly elliptical lines of equal power.

Such a weight function when used in equation 5 would produce a filter in vector wave number space that would act like a fairly sharp low pass filter and provide a good measurement of the synoptic scale wind. Work on the antenna pattern is in progress at the University of Kansas, and it will be possible to refine these calculations for application during Skylab.

In summary, two of the sources of variability in estimates of the mean wind for synoptic scale purposes, namely fading in the scattered signal and turbulent fluctuations in the wind over the water are both adequately averaged in the design of S193. The two sources of scatter combined produce a total scatter of, at most, 7%, except at 15°, so that two-thirds of the time a 30 knot wind would be estimated to be between 28 and 32 knots and a 40 knot wind would be estimated to be between 37 and 43 knots.

Additional Sources of Scatter for S193 Data. - The root mean square error for σ^o in db found by Bradley (1971) as given in Table I, and the scatter in Table V and Figure 14 was not all explained by fading effects and the turbulence in the wind. For both S193 and the airborne AAFE Langley Radscat, the instrumental problems due to the use of the fan beam Doppler system will not be present. There remains the problem of determining the wind velocity accurately for the areas of the ocean to be sampled by these instruments.

Unfortunately, the improved design of these two new instruments cannot be matched by an improvement in the accuracy with which the wind speed can be determined meteorologically, especially for S193. Some improvement can be obtained for experiments with the airborne instrument.

The problem of the adequate determination of the synoptic scale wind for patterns scanned by S193 as in Figure 15 has been treated in a proposal to NASA by McClain, Moore, Pierson and Talwani (1971) and by an amended proposal in which a concurrent aircraft program is described. The wind field as shown in Figure 16 ought to be smoothly varying over synoptic scale distances. Computer based procedures such as those developed by Cardone (1969) and described by Pierson (1970) can be used to smooth the wind field given by ship reports and surface atmospheric measurements so as to determine the wind. It is to be expected however that these estimates of the wind velocity will introduce considerable scatter in the regressions of σ^o values on wind velocity. Not only will the upwind and crosswind situations have to be treated, but also all possible angles between the beam and the wind direction. The data base for these studies will, however, be much greater so that the scatter will be more easily understood.

The use of S193 on Skylab has converted an instrument system, which when used on an aircraft, would be responsive to microscale effects and

therefore have concurrent measurement and sampling problems, to a true synoptic scale instrument in which the microscale is averaged out. The result may even be that winds determined by S193 will be so good that other wind measurement systems such as ship reports and anemometers on buoys will be calibrated against S193 instead of the other way around.

Other Problems of S193. - The preceding considerations have all been carried out under the assumption that the beam passes through clear air to the sea surface. There is the additional problem of determining the wind velocity through clouds and precipitation as illustrated by Figure 17. This problem has to be treated by Moore et al (1971). The essential points are that passive measurements lose contact with the sea surface when clouds are present long before the radar measurements and that the passive measurements can be used to correct the radar measurements for atmospheric cloud effects and find the wind at the surface.

Also there is the possibility that variations in radar backscatter can be caused by variations in sea surface temperature, salinity, and surface properties which produce changes in the dielectric properties of the water. These effects may have to be calibrated out. Finally, theories of radar sea return show that it depends on the entire wave spectrum and not on just the high wave number part of the spectrum. The dominant effect is from the short waves, but corrections for that part of the spectrum not in local equilibrium with the wind will have to be developed. These corrections are expected to be small, but necessary.

CONCLUSIONS

The extrapolation of laboratory and aircraft radar sea return data to spacecraft altitudes has shown, for S193 on Skylab, that fading effects will contribute very little scatter to the measurements and that the microscale turbulent fluctuations in the wind will be averaged out. The result should be very stable estimates of the synoptic scale winds.

Additional sources of scatter in the aircraft program were identified as being instrumental, associated with the fan beam Doppler radar that was used and the anemometer location on Argus Island, and meteorological and oceanographic. The radar problems will not be present for S193. There will still be problems in defining the wind by means of meteorological measurements to comparable accuracies.

Other problems, unique to a space instrument, such as making measurements through clouds and precipitation were identified. Methods for their solution were given.

The volume, and the improved quality, of the data from S193 should make it possible to meet the scientific objective for S193 which is to prove conclusively that simultaneous measured values of the radar scattering cross section matrix and the microwave temperature for two different polarizations at 13.9 GHz will provide data from which the winds in the planetary boundary layer over the oceans can be inferred.

ACKNOWLEDGEMENTS

The research upon which this report is based was supported by the Remote Sensing Oceanography Group of the Naval Research Laboratory under Contract N62306-70-A-0075.0007 at New York University and by generous support from several contracts and grants from NASA at the University of Kansas. The authors wish to acknowledge the contributions to this paper of many of their co-workers at Kansas and New York Universitites as indicated by their names as authors and co-authors of reports and papers cited in the references. Our thanks are also due to Mr. Duncan Ross who checked the Argus Island anemometer and obtained the anemometer data continuously during Mission 119.

Contribution No. 125, Geophysical Sciences Laboratory, New York University, Department of Meteorology and Oceanography.

REFERENCES

Baer, L. and G.W. Withee, 1971a: A methodology for defining an operational synoptic temporal oceanic sampling system I stationary conditions. J. Appl. Meteor., Vol. 10, No. 6, pp. 1053-1060.

_____, 1971b: A methodology for defining an operational synoptic temporal oceanic sampling system II non-stationary conditions. J. Appl. Meteor., Vol.10, No. 6, pp. 1061-1065.

Blackman, R.B. and J.W. Tukey, 1958: The measurement of power spectra from the point of view of communications engineering. Bell System Tech. Journ., January and March, Vol. 37, [also in book form, Dover, New York].

Bradley, G.A., 1971: Remote sensing of ocean winds using a radar scatterometer. Tech. Report 177-22, The University of Kansas Center for Research, 191 pp.

Cardone, V.J., 1969: Specification of the wind field distribution in the marine boundary layer for wave forecasting. Geophysical Sciences Lab. Report TR-69-1, New York University.

DeLeonibus, P.S., 1971: Momentum flux and wave spectra observations from an ocean tower. J. Geophys. Res. Oceans and Atmospheres, Vol. 76, No. 27, pp. 6506-6527.

Druyan, L.M., 1971: Objective analysis of sea level winds and pressures derived from simulated observations of a satellite radar radiometer and actual conventional data. Geophysical Sciences Lab. Report TR-71-7, New York University.

Lumley, J.L. and H.A. Panofsky, 1964: The structure of atmospheric turbulence. Monographs and Texts in Physics and Astronomy, Vol. XII, Interscience Publishers, John Wiley and Sons.

Lappe, U.O., B. Davidson and C.B. Notess, 1959: Analysis of atmospheric turbulence spectra obtained from concurrent airplane and tower measurements. Inst. Aero. Sci. Report No. 59-44.

McClain, E.P., R.K. Moore, W.J. Pierson and M. Talwani, 1971: A joint meteorological oceanographic geodetic and sensor evaluation program for experiment S193 on Skylab. Proposal submitted to NASA.

McDonald, J.A. and E. Herrin, 1971: The nature of turbulence. Dallas Geophysical Lab., Southern Methodist University, Dallas, Texas, August 1971, 73 pp.

Millard, R.C., Jr., 1968: Wind measurement from buoys: a sampling scheme. Unpublished manuscript, Woods Hole Oceanographic Institution, Contract ONR NR 083-004.

Mollo-Christensen, E.L. and J.R. Seesholtz, 1967: Wind tunnel measurements of the wind disturbance field of a model of the Buzzard's Bay entrance light tower. J.Geophys. Res., Vol. 72, pp. 3549-3556.

Moore, R.K. and W.J. Pierson, 1971: Worldwide oceanic wind and wave predictions using a satellite radar radiometer. J. of Hydronaut., Vol.5, No. 2, pp. 52-60.

Moore, R.K., J.P. Claassen, A.K. Fung, S. Wu and H.L. Chan, 1971: Toward RADSCAT measurements over the sea and their interpretation, in Advanced Applications Flight Experiments Principal Investigators' Review. NASA Langley Research Center, pp. 115-140.

Neumann, G. and W.J. Pierson, 1966: Principles of Physical Oceanography. Prentice-Hall Book Co., 545 pp.

Phelps, G.T. and S. Pond, 1971: Spectra of the temperature and humidity fluctuations and of the fluxes of moisture and sensible heat in the marine boundary layer. J. Atmos. Sci., Vol. 28, No. 6, pp.918-928.

Pierson, W.J., 1970: The integration of remote sensing data into global weather prediction, wave forecasting, and ocean circulation computer based systems, in Hydrology and Oceanography Third Annual Earth Resources Review, Vol. III, pp. 70-1 to 70-27.

Pierson, W.J. and V.J. Cardone, 1971: Radar satellite oceanography and ocean dynamics, (Final Report on Contract N62306-70-A-0075, Task Order .0005 with supplemental material on Task Order .0007 for the period 1 July 1970 to 1 December 1971), New York University, School of Engineering and Science.

Pierson, W.J., F.C. Jackson, R.A. Stacy, and E. Mehr, 1971: Research on the problem of the radar return from a wind roughened sea, Advanced Applications Flight Experiments Principal Investigators' Review, October 5-6, 1971, NASA Langley Research Center, pp. 83-114.

Pond, S., G.T. Phelps, J.E. Paquin, G. McBean, and R.W. Stewart, 1971: Measurement of the turbulent fluxes of momentum, moisture, and sensible heat over the ocean. J. Atmos. Sci., Vol. 28, No. 6, pp. 901-917.

Thornthwaite, C.W., W.J. Superior, and R.T. Field, 1965: Disturbance of air flow around Argus Island Tower near Bermuda. J. Geophys. Res., Vol. 70, No. 24, pp. 6047-6052.

Van der Hoven, I., 1957: Power spectrum of horizontal wind speed in the frequency range from 0.0007 to 900 cycles per hour. J. Meteorol., Vol. 14, pg. 160.